MICHIGAN STATE UNIVERSITY

CYCLOTRON LABORATORY

# A STUDY OF $^{206}Pb$ BY INELASTIC SCATTERING of 35 MeV PROTONS

J.E. FINCK, G.M. CRAWLEY, J.A. NOLEN, Jr.
and R.T. KOUZES

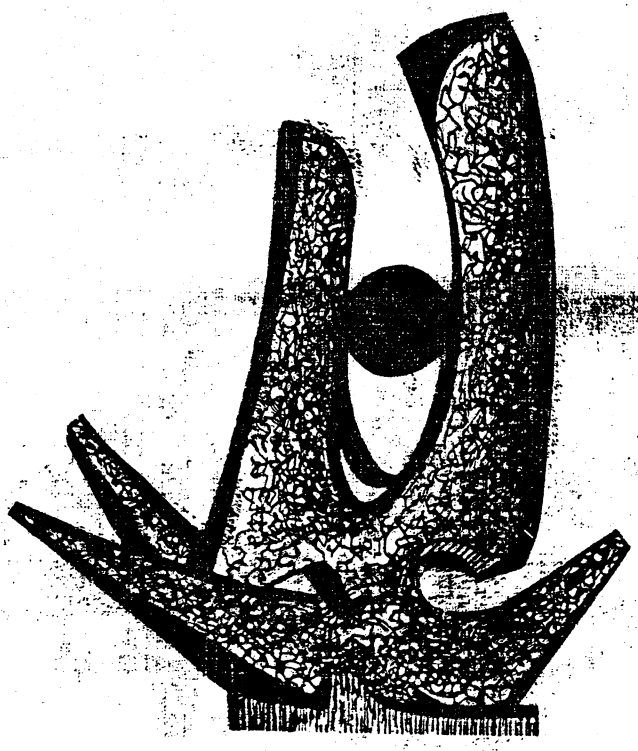

DECEMBER 1982

MSUCL-391

MSUCL-391
December 1982



# A Study of $^{206}$Pb by Inelastic Scattering of 35 MeV Protons*

J.E. Finck†

Physics Department, Northern Michigan University

Marquette, Michigan 49855

and

G.M. Crawley and J.A. Nolen, Jr.

Cyclotron Laboratory, Michigan State University

East Lansing, Michigan 48824

and

R. T. Kouzes

Department of Physics, Princeton University

Princeton, New Jersey 08544

*Supported by NSF Under Grants No. PHY80-17605 and PHY81-05673

†Present address: Physics Department, Central Michigan University, Mt. Pleasant, Michigan 48859.

## ABSTRACT

Using high resolution techniques the inelastic scattering of 35 MeV protons by $^{206}$Pb is measured. Approximately 180 levels with excitation energies up to 6.8 MeV are identified and angular distributions of most of these states are measured. L-transfers and deformation parameters are determined by comparison of the measured angular distributions to collective model calculations. Microscopic calculations of natural parity states are presented and allow a test of RPA and TDA wave functions. Unnatural parity states are also studied microscopically and permit an examination of the central and noncentral forces in the effective interaction.

## 1. Introduction

The lead region has always been an attractive area to test nuclear models. Nuclei in this mass region have been studied both experimentally and theoretically, with the bulk of this work being concerned with the structure of the doubly-magic nucleus $^{208}$Pb. Many of these studies have also extended to the single-hole structure of $^{207}$Pb and the single-particle structure of $^{209}$Bi which are now well-established. An examination of $^{206}$Pb is a further step toward the more complex structure that exists away from closed shells.

Experiments previously performed on $^{206}$Pb include inelastic scattering [1-3] which has given information about the strongly excited states. Information about the microscopic structure of many of the low-lying states has been provided by decay studies [4-6], transfer reactions [7-10], and isobaric analog resonance experiments [11,12]. The spins and parities of many higher-lying levels have also been determined by these experiments. Using the shell model which describes $^{206}$Pb as two neutron holes in the $^{208}$Pb core, energies and wave functions of the low-lying levels of $^{206}$Pb have been calculated [13,14]. With this background a detailed study of inelastic proton scattering from $^{206}$Pb, including collective and microscopic calculations, has been undertaken.

A proton inelastic scattering experiment on $^{206}$Pb has been reported [1-3] at 24.5 MeV bombarding energy with an energy resolution of approximately 25 keV. This experiment identified approximately 30 levels, and spin and parity assignments for the most strongly excited states were made. Using collective model calculations, the reduced transition rates for some of these states were extracted, and the angular distributions were compared with the collective model predictions.



Only states below 4.6 MeV were observed and weakly excited states in this region were not observed. This represents the most extensive study of $^{206}$Pb(p,p') to date.

This paper reports a study of $^{206}$Pb(p,p') performed at 35 MeV with an energy resolution of 6 to 20 keV. Approximately 180 levels of $^{206}$Pb with excitation energies up to 6.8 MeV are observed. Measured angular distributions for 144 of these levels are presented. The collective model is used in fitting many of these angular distributions, and L-assignments and deformation parameters are obtained for these states. Microscopic calculations are performed for a number of natural and unnatural parity states. The microscopic examination of natural parity states permits the testing of wave functions since such transitions depend little on the noncentral two-body interaction. Wave functions obtained from the random phase and Tamm-Dancoff approximations are examined. Unnatural parity transitions to levels with well-determined wave functions allow the two-body central, tensor, and spin-orbit forces to be studied. In this study two different sets of forces are employed for comparison with experimental results.

## 2. Experimental procedure

The experiment was performed using 35 MeV proton beams from the Michigan State and Princeton University cyclotrons. Targets of 0.1 mg/cm$^2$ thickness enriched to 97.22% were prepared by vacuum evaporation on a 20 mg/cm$^2$ carbon foil with a support of two layers of Formvar. To assure relative normalization the data were monitored with a NaI(Tl) detector placed at an angle of 90$^o$ relative to the incident beam.

The spectra recorded in this experiment were obtained using nuclear emulsions in the focal plane of the Michigan State University Enge split-pole magnetic spectrograph, as well as a position-sensitive proportional counter in the focal plane of the Princeton University QDDD spectrograph. A stainless steel absorber of thckness 0.25 mm was placed immediately before 10 inch Kodak NTB 25 μm nuclear emulsions. The absorber stopped all particles other than protons, and decreased the proton energy. This enhanced the proton tracks in the emulsion and did not significantly broaden the line width. On-line determination of the focal plane line width was optimized by adjusting the dispersion of the beam across the target using a "speculator" technique [15]. Once the dispersion was optimized, the resolution remained constant throughout the experiment. The resolution of the plate data ranges from 6-9 keV (FWHM). A typical spectrum of plate data is shown in Fig. 1. States of well-determined spin and parity have been identified. Each plate run covers excitation energies from the ground state to about 7.0 MeV. Some strongly excited states, such as the 3$^-$ state at 2.648 MeV of excitation, produce tracks too dense to scan.



Data with the proportional counter were recorded in three passes covering the energy range from the ground state up to 5.5 MeV of excitation. The energy resolution of these data is 15 to 20 keV. Data at 40$^o$, taken in three segments, are displayed in Fig. 2. The only counter data used in the analysis in this paper are states labeled in these spectra.

Both methods of acquiring data offer unique advantages. Data taken with the nuclear emulsions have far better resolution allowing weakly excited and close lying states to be analyzed. The linearity of the plates yields accurate excitation energies. The proportional counter gives more accurate cross section data for strongly excited states because it is not limited by the number of counts in a peak. Because energy resolution is not as crucial in this part of the experiment, a comparatively large solid angle could be used and data were accumulated at a rapid rate.

## 3. Results

Listed in Tables 1 and 2 are the excitation energies of the approximately 180 levels of $^{206}$Pb observed in this experiment. In Table 1 the levels with excitation energy below 4.6 MeV are compared with the results of a recent compilation [16] and an inelastic proton scattering experiment [2] with an incident proton energy of 24.5 MeV. Above 4.6 MeV of excitation the correspondence of levels seen in different reactions is uncertain due to the high level density and uncertainty of excitation energy. As a result the data in this region, displayed on Table 2, are not compared with previous results. All levels listed in these tables were clearly observed in the photographic plate data at a minimum of three angles. The energy calibration of each plate exposure was determined using both $^{206}$Pb states and well-known levels of nuclei which were present as impurities in the target. The $^{206}$Pb states used had focal plane positions clearly determined in this experiment, and had excitation energies established in other high resolution experiments [7,8,17,18]. These calibration states are indicated in Table 1. The levels of $^{12}$C and $^{16}$O, as well as the ground states of $^{35}$Cl and $^{37}$Cl were used whenever possible. The excitation energies given in Tables 1 and 2 include statistical uncertainties plus an additional error of 1 keV per 500 keV of excitation energy for states beyond 3.5 MeV of excitation energy. This systematic error is an estimate of both the interpolation error and the uncertainties in the peak positions caused by the high level density.

Below about 4.6 MeV of excitation energy most states are well-resolved and the agreement with previous work is very good. Several new levels have been



identified in this region including two relatively strongly excited states at 3.257 and 3.980 MeV of excitation energy. A level previously reported at 2.658 MeV [16] is not observed. Even if this level is excited in the present experiment it could not be resolved from the state at 2.648 MeV of excitation energy in the counter data, and because the 2.648 MeV state is the strongest excited state in this reaction the particle density is too intense to analyze in the plate data. Other levels previously reported in this region, yet not seen in this experiment, are probably weakly excited, and an upper limit of 10 μb/sr can be put on their maximum cross section.

Angular distributions for inelastic states seen at four or more angles are shown in Figs. 3 through 5. The cross sections are displayed with their corresponding excitation energies. Error bars indicate statistical errors and are drawn only when greater than the symbol size. The curves drawn through the data are included as guides to the eye and do not represent theoretical fits to the data.

## 4. Collective model analysis

For comparison with the measured angular distributions, distorted wave Born approximation calculations were performed using the computer code DWUCK [19]. The optical model parameters used in the analysis are the general set of Becchetti and Greenlees [20]. A comparison of the measured elastic scattering angular distribution with a calculation using these parameters is shown in Fig. 6. Since the target thicknesses were known only approximately, the normalization of elastic scattering to this calculation is used to determine the values for the thickness of the different targets. Using this procedure the absolute cross sections are believed to be accurate within 10%.

Angular distributions for natural parity states are very characteristic of the angular momentum transfer. Comparisons of collective model fits to identified states are displayed in Figs. 7 and 8 and discussed below. The L-transfers are determined by comparing the data with theoretical angular distributions, and experimental cross sections of states with unambiguous L-assignments. The experimental cross sections used in this comparison to aid in L-assignments include both $^{206}$Pb states observed in this experiment and $^{208}$Pb states observed in the 35 MeV proton study by Wagner et al [21]. Deformation parameters were obtained from $\beta_L^2 = {}^{\sigma}\mathrm{exp.}/{}^{\sigma}\mathrm{Th.}$ The deformation parameters and L-transfer assignments of levels below 4.6 MeV of excitation are given in Table 1 for comparison with the measurements of References 2 and 16. Where possible those states with angular distributions of unidentifiable shape have $J^{\pi}$ adopted from Reference 16. The L-assignments and deformation parameters of levels above 4.6 MeV are given in Table 2.



The deformation parameter $\beta_L$ is used to determine the reduced transition probability $G_L$ in single particle units (s.p.u.). This relation is given by:

$$G_L = \frac{(3+L)^2}{4\pi(2L+1)} Z^2 \beta_L^2,$$

where Z is the atomic number of the target.

Another quantity of interest is the fraction of the energy-weighted sum rule (EWSR) limit for a particular multipole contained in the observed transitions. The sum of the observed energy weighted transition strength is given by:

$$S_L = \sum_f G_{L_f} E_f$$

where the sum is taken over all final states f of energy $E_f$ reached by a particular multipolarity L.

### 4.1 L=2 TRANSITIONS

Six probable quadrupole states were observed. These states have 17% of the total expected strength given by an EWSR. Most of the L=2 strength is concentrated in the first excited state at 0.803 MeV and a state at 4.107 MeV. These two states have transition strengths of 1.7 and 5.9 s.p.u. respectively. A well known $2^+$ state at 1.469 MeV was observed. The excitation energy of this state is not in agreement with decay studies [22] but is consistent with the energy measured in transfer reaction experiments [7]. The states at 2.151 and 2.422 MeV were previously assigned a $J^{\pi}$ value of $2^+$. These levels are observed to be weakly excited in the present experiment but their angular distributions do show the characteristic L=2 shape. A state at 4.242 MeV was previously identified as a $5^-$ state [10]. This experiment suggests an assignment of L=2.

Inelastic proton scattering from $^{208}$Pb [21] also identified six L=2 states with approximately the same total strength. However, all six states observed in $^{208}$Pb had energies above 4 MeV of excitation.

4.2. L=3 TRANSITIONS

Previous experiments have only definitely identified one $3^-$ state, at 2.648 MeV of excitation. Two other states at 5.444 and 6.045 MeV of excitation were tentatively assigned a $J^\pi$ value of $3^-$ [10]. The 2.648 MeV level is the strongest excited state observed in the present experiment with a transition strength of 32.1 s.p.u. exhausting about 18% of an EWSR. The $3^-$ strength is fractionated and many other states with a characteristic L=3 shape were observed. In particular, the levels at 3.718 and 5.245 MeV are relatively strongly excited. The angular distribution of the 5.092 MeV state is fit equally well with L=3 or L=4 shapes so that the L-transfer is not uniquely determined. The observed $3^-$ states have 36% of the total expected strength given by the EWSR.

4.3. L=4 TRANSITIONS

The dominant $4^+$ state observed was the 4.333 MeV level with a transition strength 8.8 s.p.u. The other well-known levels at 1.686, 1.998, and 2.928 MeV were observed with transition strengths of 2.6, 0.8, and 2.6 s.p.u. respectively. New $4^+$ states were identified which were not previously reported, notably the relatively strongly excited (>1 s.p.u.) states at 3.450, 5.007, 5.422, 5.561, and 5.911 MeV of excitation. There is some ambiguity in assigning the levels at 4.710 and 5.796 MeV since both of these levels could probably be equally well fit by an L=5 shape. The observed $4^+$ states have 24% of the expected strength given by the EWSR.

4.4. L=5 TRANSITIONS

All known $5^-$ states were observed, the strongest being the state at 3.772 MeV of excitation with 5.8 s.p.u. of transition strength. Previously unreported levels at 4.456, 4.793 and 5.588 MeV are all relatively strongly excited. The L=5



assignment to the level 3.515 MeV is in disagreement with the tentative $3^+$ or $4^+$ assignment of Reference 8. This angular distribution is not fit well by an L=5 shape before the first maximum at 37 degrees, which can be seen in Fig. 8. On the basis of this fit an assignment of L=5 seems rather weak. However, it has been previously noted [22] that the predicted collective model cross section for large angular momentum transfer usually underestimates the forward angle data. This difference between data and theory is amplified as the spin of the state increases. An example of similar behavior can be observed by examining two well-known $5^-$ states in $^{206}$Pb at 2.782 and 3.277 MeV. Both states show this phenomena where forward angle data tend to rise relative to the calculation. Indeed the shape of the measured 3.277 MeV state is nearly identical to the state in question. As a result of the similarity of the 3.515 MeV state with established levels it has been tentatively assigned to be an L=5 transition.

4.5. L=6 TRANSITIONS

The only previously observed L=6 level seen in this experiment is the strongly excited state at 4.357 MeV with 9.7 s.p.u. of transition strength. New L=6 levels observed include relatively strongly excited states at 3.257, 4.123, and 4.939 MeV.

4.6. L>7 TRANSITIONS

Only two states were identified as involving L=7 transitions. The established level at 2.200 MeV was identified with 1.7 s.p.u. of transition strength and a previously unidentified state at 4.828 MeV is tentatively assigned an L=7 shape with transition strength of 1.9 s.p.u. Transfer reaction experiments [7,8] have found more L=7 strength in $^{206}$Pb, and levels at similar excitation energies were observed in this experiment. However, these states are weakly excited and their angular distributions do not contain enough information to make reasonable L-assignments.

Two $8^+$ states were observed with the strongest being the level at 4.580 MeV. This state has a transition strength of 4.2 s.p.u.

## 4.7. SUMMARY OF THE COLLECTIVE MODEL RESULTS

Almost one hundred-fifty angular distributions have been measured in the present $^{206}$Pb (p,p') experiment. For half of these transitions, L-values have been determined using a macroscopic DWBA analysis. At excitation energies below about 4 MeV previous studies have identified most of the levels and the results of this experiment agree quite well with these earlier results. A few new levels in this region have been identified in this experiment. Most of the L-assignments for states above 4 MeV of excitation were previously unreported.

The results of this collective model analysis are presented in Fig. 9 and are compared with the results of a similar experiment on $^{208}$Pb [21]. Here the strength of each L-transfer has been displayed according to excitation energy. This comparison shows a definite correlation in both energy and relative strength of the five strong collective $3^-$, $2^+$, $4^+$, $6^+$, and $8^+$ states in the two nuclei. In addition, the distribution of L=3 inelastic strength is quite similar in the two nuclei. This suggests that the octupole strength in the lead region is rather insensitive to the $p_{1/2}$ neutron population. However, the distribution of inelastic strength in $^{206}$Pb and $^{208}$Pb is quite different for the other L-transfers. In $^{208}$Pb all the L=2, L=4, L=6 and L=7 strength is above 4 MeV of excitation. In $^{206}$Pb, however, there is a significant excitation of all these L-transfers below 4 MeV. The L=5 strength is quite fractionated in $^{206}$Pb, especially below 4 MeV of excitation.



## 5. Microscopic model

Shell model calculations for $^{206}$Pb [23,24] predict a number of states with unnatural parity. Since macroscopic DWBA calculations only describe collective excitation of states it is not expected that the angular distributions of these levels can be described by such a model. Therefore, we performed microscopic calculations for identified unnatural parity states and a number of low-lying natural parity states to investigate the microscopic structure and the associated reaction mechanism for exciting these states.

The microscopic calculations were performed with the code DWBA-70 of Schaeffer and Raynal [25]. The code allows the treatment of real interactions with central, tensor, and spin-orbit components, and an exact treatment of "knock-on" exchange. In this study two different forces are employed for comparison to experimental results. The first set of interactions (Force A) uses the Serber exchange mixture for the central part of the interaction. The tensor force was taken from the works by Crawley et al [26], and by Fox and Austin [27]. The L·S force was taken from studies by Fox and Austin [27]. This set of interactions was used in a previous study of $^{208}$Pb (p,p') by Wagner et al [21].

The second set of interactions (Force B) is from calculations by Bertsch et al [28]. This force is derived by fitting to the harmonic oscillator matrix elements of the Reid or Hamada and Johnson nucleon-nucleon potentials. Several choices for the individual terms in the interaction are given in Ref. 28. The present calculations have utilized the sum of the interactions labeled 1, 4, 11, 14, 16, and 18 in Table 1 of that paper. This set is obtained mostly from the Reid interaction, and is the set preferred by the authors of Ref. 28. Similar sets of

interactions were previously utilized in a study of 40 MeV protons inelastically scattered from $^{24}Mg$ [29], and in a study of unnatural parity states of $^{88}Sr$ excited by 17.2 MeV protons [30]. The latter study is of particular interest here because $^{88}Sr$, being two protons removed from the doubly magic-nucleus $^{90}Zr$, is similar in strucutre to $^{206}Pb$, which is two neutrons removed from the doubly-magic nucleus $^{208}Pb$.

The wave functions of the low-lying levels of $^{206}Pb$ are described by two neutron holes in the $^{208}Pb$ core. Shell model calculations based on these two interacting neutron holes have been performed for $^{206}Pb$ with both the Tamm-Dancoff approximation (TDA) and the random phase approximation (RPA). In the present microscopic calculations wave functions derived from both methods are utilized. The TDA wave functions have been obtained from the work of True and Ma [23], who employ phenomenological nucleon-nucleon interaction of a Gaussian central force plus a weak-coupling force, with a conventional shell-model calculation. RPA wave functions come from the work of Vary and Ginocchio [24] who use a central interaction. In general the energies predicted by the TDA are in slightly better agreement with experimental results than the RPA predictions. However, electromagnetic transition rates are given more accurately with the RPA.

Microscopic calculations of angular distributions predicted by these theoretical wave functions are shown in Figs. 10 through 13. Both direct and direct-plus-exchange calculations are presented. An asterisk indicates the direct calculation. For these microscopic calculations, the results with Force A are given by the solid curves while the dashed curves indicate results using Force B.

## 5.1. NATURAL PARITY STATES

Considered first are states of normal parity lying below the dominant $3^-$ level at 2.648 MeV. Displayed in Fig. 10 are cross sections predicted by the RPA



wave functions of the first excited $0^+$ state, the first five $2^+$ states, the first two $4^+$ states and the first $7^-$ state. The strongest state in this region of excitation is the first excited state of $^{206}Pb$, the $2^+$ state at 0.803 MeV. The shape of this angular distribution is reproduced well by the calculation. However, its magnitude is underestimated by about a factor of three. Levels of moderate strength in this region of excitation energy include the $2^+$ state at 1.469 MeV, both $4^+$ states, and the $7^-$ state. The shape and strength of these angular distributions are very well reproduced, especially by the calculations using Force B. In general Force B does better than Force A in matching the magnitude of the angular distributions and in reproducing the shape of these states of moderate strength. The success of Force B is especially clear at forward angles. The weakly excited $2^+$ state at 2.151 MeV of excitation is best fit by Force A. The remaining weak $0^+$ state and $2^+$ states are overestimated by these calculations, however, the shapes are well reproduced in general.

Figure 11 shows measured angular distributions of these same low-lying natural parity states compared with microscopic calculations using TDA wave functions. The $2^+$ state at 0.803 MeV is underestimated by about an order of magnitude. The data for the collective 1.686 MeV $4^+$ level is also stronger than predicted. In general the angular distributions of these states calculated using the TDA wave functions reproduce the weakly excited states as well as the RPA calculations, but give poorer agreement than the RPA calculations for the strongly excited states. Examining the wave functions in detail reveals some differences between the RPA and TDA predictions. For all the $2^+$ states, the $0^+$ state and the $7^-$ state examined here, the main particle-hole component is consistently larger in the RPA wave functions. This results in an improved fit for all these levels except the $0^+$ state. This suggests that these states are excited primarily in a single particle-hole configuration, and that the $0^+$ is probably a mixture of particle-hole components.

There is a major discrepancy between the predicted wave functions for the two $4^+$ states. Both the TDA and the RPA predict these $4^+$ states to have a configuration which is a combination of the $|f_{5/2}, f_{5/2}^{-1}>$ and $|f_{5/2}, p_{3/2}^{-1}>$ neutron particle-hole components. One of these components is always paramount while the second is of moderate strength. Other particle-hole components contribute only modestly to these wave functions. The RPA predicts the configuration of the $4^+$ state at 1.686 MeV to be dominated by the $|f_{5/2}, f_{5/2}^{-1}>$ component, while the $4^+$ state at 1.998 MeV is dominated by the $|f_{5/2}, p_{3/2}^{-1}>$ configuration. The TDA wave functions for these two states have the same combinations of these particle-hole components only reversed. The angular distributions of these $4^+$ states are clearly predicted better using the RPA wave functions.

Examined next are several highly collective natural parity states with excitation energies around 3 MeV. In Fig. 12 measured angular distributions of the $4^+$ state at 2.928 MeV, the $5^-$ states at 2.782 and 3.014 MeV, and the $6^+$ state at 3.257 MeV are compared with calculations using RPA wave functions. The shapes of these angular distributions are all reasonably well reproduced. The first $5^-$ state and the $4^+$ state are underestimated by the calculations. The magnitudes of the second $5^-$ state and the $6^+$ state are accurately predicted by the calculations, especially by Force A. Shown in Fig. 13 are calculated angular distributions of these states using TDA wave functions. These wave functions yield very different results. With the exception of the second $5^-$ state, the predicted magnitudes fall far short of the data, by as much as a factor of 30 in the case of the $6^+$ state. As was the case with some of the low-lying states the systematic difference between the two sets of wave functions is the RPA wave functions have a larger concentration of strength in the principal particle-hole component. Here also is another major difference between the two sets of wave functions. The TDA predicts the largest neutron particle-hole component for the $6^+$ state to be $|f_{5/2}, f_{7/2}^{-1}>$. The corresponding



RPA wave function predicts this state to be an essentially pure $|_{9/2}, g_{9/2}^{-1}>$ particle-hole state.

In Fig. 14 the measured angular distributions of the $2^+$ state at 1.469 MeV and the $4^+$ state at 1.686 MeV are compared with angular distributions using Force A and Force B. Calculations using the total forces are presented, and the force is broken down to show the contributions of the central and noncentral component parts independently. The calculations show clearly that the angular distributions of these natural parity states predicted by the total forces are dominated by the central part. For both states the central force is predicted to be larger using Force B. This increased central contribution results in a calculation with the complete Force B which is about fifty percent stronger than the calculation using Force A. Although the noncentral forces contribute weakly, it is instructive to note that the shapes of the tensor and spin-orbit calculations using Force A and Force B are very similar, and the predicted magnitudes are nearly the same.

## 5.2. UNNATURAL PARITY STATES

When examining the natural parity states it is difficult to infer more than general information about the interactions. This problem is due to both the uncertainty in the wave functions of these states, and possible excitation of these states by collective modes. However, unnatural parity states pose no such problem. Three low-lying unnatural parity states have been firmly identified [16] and both the RPA and TDA predict these to be pure neutron particle-hole states. These three states are the $3^+$ state at 1.344 MeV, the $1^+$ state at 1.708 MeV, and the $6^-$ state at 2.385 MeV. The neutron particle-hole configuration of these states is respectively $|p_{1/2}, f_{5/2}^{-1}>$, $|p_{1/2}, p_{3/2}^{-1}>$, and $|p_{1/2}, i_{13/2}^{-1}>$. Calculated angular distributions using both Force A and Force B, and broken down into their central and noncentral constituent parts, are compared to the data in Fig. 15.

The calculations using Force A reproduce the general shape of the data but the magnitudes of the $3^+$ and $1^+$ levels are underestimated by about a factor of three. The data of the $6^-$ state falls off more rapidly than the calculation predicts. For all three states the tensor part of Force A is the dominant interaction. The central force is the weakest interaction and its contribution to the total predicted angular distribution is observed to be less significant as the total angular momentum of the states examined increases. The only significant contribution by the spin-orbit force is over a limited angular range for the $1^+$ state.

When Force B is employed the predicted cross sections are all improved. The shape of the $3^+$ state is matched well and the theory underestimates the data by only about a factor of two. The enhancement of the magnitude is caused principally by the increased strength of the central part of the interaction. The central part is observed to be nearly equal in strength to the tensor part. Since these two components are out of phase, the angular distribution predicted by the complete



Force B has less structure than is predicted by Force A. Thus the prediction of Force B compares better with the data. Force B also gives an improved estimate of the magnitude of the $1^+$ state. For this state the central force dominates the tensor force at forward angles causing the total calculation to be larger than the data in this region. However, past thirty degrees, where the central and tensor parts give contributions of similar strength, the shape and magnitude are predicted quite well. The fit to the $6^-$ state using Force B approaches the slope of the data more closely than the fit obtained using Force A. Once again it is the increased strength of the central part which is responsible for the improvement. The contribution of the central part of Force B is also observed to decrease significantly as the angular momentum of the state increases. A similar phenomena is observed with Force A but to a lesser degree. The predicted shape and magnitude of the spin-orbit interaction with both forces is similar for all states.

In addition to the three established unnatural parity states there is evidence for two more unnatural parity states which should be seen in this experiment. A $3^+$ state with a pure $|p_{1/2}, f_{7/2}^{-1}>$ neutron particle-hole configuration is predicted at 3.193 MeV of excitation energy by the TDA, and at 3.156 MeV of excitation by the RPA. The level observed at 3.121 MeV has been suggested by a (p,d) experiment [8] to be this $3^+$ state. The RPA also predicts a $1^+$ state with a $|f_{5/2}, p_{3/2}^{-1}>$ configuration at 3.963 MeV of excitation. Two $1^+$ states are predicted by the TDA at 2.317 and 3.759 MeV of excitation energy with pure $|f_{5/2}, p_{3/2}^{-1}>$ and $|f_{5/2}, f_{7/2}^{-1}>$ configurations, respectively. The state observed in this experiment at 3.737 MeV has been shown [16] to be a possible candidate for a $1^+$ state.

Angular distributions for these two possible unnatural parity states have been calculated with both forces. The results are displayed in Fig. 16. The magnitude of the 3.121 MeV state is underestimated especially at forward angles by Force A which excites this state principally by the tensor part of the force. The calculation done with Force B is somewhat better in reproducing the magnitude. However,

the fit at forward angles is still poor. The improved fit is caused by both a slightly larger contribution by the tensor part and a contribution by the central part that is nearly an order of magnitude larger than the central force contribution of Force A.

The calculations performed for the $1^+$ state have used the configuration proposed by the RPA. This state lies on the shoulder of a relatively strongly excited L=3 state and is extracted at only a few angles. As a result it is difficult to compare predicted shapes of the angular distributions to the data, but there is enough information to suggest that the magnitude of this state is best reproduced with Force B.



## 5.3. SUMMARY OF THE MICROSCOPIC MODEL RESULTS

Microscopic calculations were performed on most low-lying natural parity states and all unnatural parity states identified in this experiment. These calculations were executed with the program DWBA-70 using realistic interactions and shell model wave functions. "Knock on" exchange contributions to the cross sections were included. The calculations allowed a test of wave functions predicted by the Tamm-Dancoff approximation and the random phase approximation. Two realistic interactions were employed and compared. Force A used the Serber exchange mixture for the central force, and empirically determined noncentral forces. Force B was derived by fitting to the harmonic oscillator matrix elements of the Reid potential.

Natural parity states with peak cross sections $\gtrsim$0.1 mb/sr were best fit with Force B. These states were shown to be excited principally by the central part of the interaction, and the central contribution of Force B is as much as fifty percent larger than the central contribution of Force A. The tensor and spin-orbit forces gave little enhancement to the cross sections of natural parity states. The predicted shapes using either force or wave function were found to be very similar to the measured angular distributions. These natural parity states were in general reproduced best with the RPA wave functions. In all cases where the predicted wave functions were significantly different, the RPA clearly gave a better fit to the data. Furthermore, it was observed that the RPA wave functions for most of these states had a larger concentration of strength in the primary particle-hole component. With the exception of the $0^+$ excited state this tended to improve all predicted angular distributions. This suggests that these states may be described by a rather simple single particle-hole configuration.

Unnatural parity states are not excited collectively and the wave functions of these states are predicted by both the RPA and TDA to have simple single particle-hole configurations. Thus, calculations of these states permit a unique examination

of the forces. With Force A calculations of all observed unnatural parity states underestimate the magnitude of the data, while generally reproducing the shape. The calculations have shown that only the tensor part of Force A gave a substantial contribution to the predicted cross section. The results obtained with Force B were all much better. This improvement is caused to some degree by a small increase in the tensor strength for all states, but mainly because of a contribution by the central part which is similar in magnitude to the tensor force. This central force was seen to be most influential for the lower spin states. The resulting calculations using central and noncentral interactions in general match the magnitude of the data reasonably well. This central force also added to the tensor force in such a way as to smooth out the structure in the calculated angular distribution and thus give better agreement with the data.



## 6. SUMMARY

The measurement of the inelastic scattering of 35 MeV protons from $^{206}Pb$ has allowed identification of approximately 180 levels. Below 4.6 MeV of excitation energy the agreement with previous studies is very good, and several new states were observed in this region. Many new levels above 4.6 MeV were also measured. Angular distributions are presented for 144 of these states.

Angular distributions predicted by the collective and microscopic models are compared to the data. The collective model calculations allowed the extraction of L-values and deformation parameters. For states where results from other studies were available the agreement is quite good. The L-assignments for most states of high excitation energy were previously unreported. The collective model results for $^{206}Pb$ were also compared to the core nucleus $^{208}Pb$. This comparison showed a similarity between the two nuclei for the L=3 strength and for some individual strongly excited states of different multipolarity. However, the overall distribution of inelastic strength was quite different for multipolarities other than L=3.

Microscopic calculations performed on natural parity states indicated that these states were excited primarily by the central two-body interaction. RPA and TDA wave functions were tested in calculations. The RPA wave functions, which gave the best fit to the data, suggested that many of the states examined have primarily a single particle-hole configuration. Microscopic calculations for unnatural parity states with well determined wave functions permitted more detailed examination of the two interactions. The magnitude and shape of the angular distributions of these states was best represented using Force B. This force predicted the central and tensor parts of the interaction to be similar in magnitude.

It would be of interest to study inelastic scattering of protons by $^{206}Pb$ at higher energies. Based on the apparent simple wave functions of many states in $^{206}Pb$, this nucleus provides an ideal target to examine the energy dependence of the central, tensor, and spin-orbit forces. Also of interest would be a study similar to the present work on $^{88}Sr$. Inelastic proton scattering by $^{88}Sr$ at 17.2 MeV has been previously studied [32] This report examined the low-lying $1^+$ and $3^+$ states and described the excitation of these states by very simple wave functions. The wave functions were analogous to those used in the present work to describe the low-lying $1^+$ and $3^+$ states of $^{206}Pb$.



REFERENCES


1) J. Saudinos, G. Vallois, and O. Beer, Nucl. Sci. Appl. 3 (1967) 22.
2) G. Vallois, J. Saudinos, and O. Beer, Phys. Lett. 24B (1967) 512.
3) G. Valois, Centre d'Etudes Nucleaives de Saclay, Report CEA-R3500 (1968).
4) J. C. Manthuruthil, D. C. Camp, A. V. Ramayya, J. H. Hamilton, J. J. Pinajian, and J. W. Doornebos, Phys. Rev. C 6 (1972) 1870.
5) J. E. Draper, R. J. McDonald, and N. S. P. King, Phys. Rev. C 16 (1977) 1594.
6) D. F. Coope, L. F. Cannell, and M. K. Brussel, Phys. Rev. C 15 (1977) 1977.
7) W. A. Lanford, Phys. Rev. C 16 (1977) 988.
8) W. A. Lanford and G. M. Crawley, Phys. Rev. C 9 (1974) 646.
9) R. Tickle and J. Bardwick, Phys. Rev. 166 (1968), 1167.
10) E. R. Flynn, R. A. Broglia, R. Liotta, and B. S. Nilsson, Nucl. Phys. A221 509.
11) J. Solf, C. F. Moore, E. Grosse, and P. von Brentano, Nucl. Phys. A139 (1969) 523.
12) P. Richard, N. Stein, C. D. Kavoloski, and J. S. Lilley, Phys. Rev. 171 (1968) 1308.
13) W. W. True and C. W. Ma, Phys. Rev. C 3 (1971) 2421.
14) J. Vary and J. N. Ginocchio, Nucl. Phys. A166 (1971) 479.
15) H. G. Blosser, G. M. Crawley, R. de Forest, E. Kashy, and B. H. Wildenthal, Nucl. Instr. and Meth. 91 (1971) 61.
16) M. P. Webb, Nucl. Data 26, No. 1 (1979) 145.
17) M. Kanbe, M. Fujioka, K. Hisatake, Nucl. Phys. A192 (1972) 151.
18) J. C. Manthurathil, D. C. Camp, A. V. Ramayya, J. H. Hamilton, J. J. Pinajian, and J. W. Doornebos, Phys. Rev. C 6 (1972) 1870.
19) P. D. Kunz, University of Colorado, unpublished.
20) F. D. Becchetti and G. W. Greenlees, Phys. Rev. 182 (1969) 1190.
21) W. T. Wagner, G. M. Crawley, G. R. Hammerstein, and H. McManus, Phys. Rev. C 12 (1975) 757.
22) M. Lewis, F. Bertrand, and C. B. Fulmer, Phys. Rev. C 7 (1973) 1966.
23) C. W. Ma and W. W. True, Phys. Rev. C 8 (1973) 2313.
24) J. Vary, R. J. Ascuitto, and J. N. Ginocchio, Nucl. Phys. A185 (1972) 349.
25) R. Schaeffer and J. Raynal, unpublished.
26) G. M. Crawley, S. M. Austin, W. Benenson, V. A. Madsen, F. A. Schmittroth, and J. J. Stomp, Phys. Lett. 32B (1970) 92.
27) S. H. Fox and S. M. Austin, Phys. Rev. C 21 (1980) 1133.
28) G. Bertsch, J. Borysowicz, H. McManus, and W. G. Love, Nucl. Phys. A284 (1977) 399.
29) B. Zwieglinski, G. M. Crawley, W. Chung, H. Nann, and J. A. Nolen, Jr., Phys. Rev. C 18 (2978).
30) F. E. Cecil, R. P. Chestnut, and R. L. McGrath, Phys. Rev. C 10 (1974) 2425.

FIGURE CAPTIONS:

Fig. 1. Typical spectrum of protons scattered by $^{206}$Pb obtained with a photographic plate. States of well-determined spin and parity are identified. The resolution is about 6 keV.

Fig. 2. Typical spectrum of protons scattered by $^{206}$Pb obtained with the proportional counter.

Fig. 3. Measured inelastic cross sections. The lines drawn through the data points are included to guide the eye and do not represent theoretical fits to the data.

Fig. 4. Same as Fig. 3.

Fig. 5. Same as Fig. 3.

Fig. 6. Comparison of the measured elastic angular distribution with the DWBA calculation explained in the text.

Fig. 7. Collective model fits for identified states. Displayed with each fit are the excitation energy of the state and the deformation parameter, $\beta_L$, corresponding to orbital angular momentum transfer L.

Fig. 8. Same as Fig. 7.

Fig. 9. Results of collective model fits of $^{206}$Pb compared to $^{208}$Pb. The deformation parameter, $\beta_L$, is plotted against excitation energy for a number of L-transfers.

Fig. 10. Microscopic model fits for low-lying natural parity states using RPA wave functions. The solid lines correspond to calculations done with Force A; the dashed curves show results using Force B. The asterisks indicate only direct calculations. The curves without asterisks indicate calculations including exchange effects.

Fig. 11. Same as Fig. 10 with TDA wave functions used in the calculations.

Fig. 12. Microscopic Model fits for higher-lying natural parity states using RPA wave functions. The meanings of the curves and asterisks are the same as in Fig. 10.



Fig. 13. Same as Fig. 12 with TDA wave functions used in the calculations.

Fig. 14. Comparison of measured angular distributions with the central and noncentral parts of Force A and Force B.

Fig. 15. Same as Fig. 14.

Fig. 16. Same as Fig. 14.

TABLE CAPTIONS:

Table 1. Energy levels, L-transfers, and deformation parameters for $^{206}$Pb. A comparison is made with previous results.

a. All energies are in MeV.
b. Level used in energy calibration.
c. Spin and parity adopted from Ref. 16.

Table 2. Energy levels, L-transfers, and deformation parameters for $^{206}$Pb.

a. All energies are in MeV.

| Present Work | | | 24.5 MeV (p,p') Ref. 2 | | | Compilation Ref. 16 | |
|---|---|---|---|---|---|---|---|
| $E_x \pm \Delta E_x$ [a] | L | $\beta_L$ | $E_x$ [a] | L | $\beta_L$ | $E_x$ [a] | $J^\pi$ |
| 0.00[b] | | | | | | 0.00 | $0^+$ |
| 0.8031[b] | 2 | .066 | 0.803 | 2 | .068 | 0.8031 | $2^+$ |
| 1.170±.003 | | | | | | 1.1651 | $0^+$ |
| 1.344±.002 | $J^\pi=3^+$[c] | | 1.328 | | | 1.3406 | $3^+$ |
| 1.469±.002 | 2 | .015 | 1.459 | | | 1.467 | $2^+$ |
| 1.686±.001 | 4 | .030 | 1.684 | 4 | .042 | 1.6841 | $4^+$ |
| 1.708±.003 | $J^\pi=1^+$[c] | | | | | 1.703 | $1^+$ |
| 1.787±.002 | | | 1.789 | | | 1.784 | $2^+$ |
| 1.9977[b] | 4 | .017 | 1.996 | 4 | .023 | 1.9977 | $4^+$ |
| 2.151±.003 | (2) | .009 | | | | 2.149 | $(2^+)$ |
| 2.20023[b] | 7 | .022 | 2.199 | 7 | .031 | 2.20023 | $7^-$ |
| | | | | | | 2.315 | $0^+$ |
| | | | | | | 2.379 | |
| 2.385±.002 | $J^\pi=6^-$[c] | | 2.381 | | | 2.3843 | $6^-$ |
| | | | | | | 2.3914 | |
| 2.422±.003 | (2) | .006 | | | | 2.424 | $2^+$ |
| 2.6479[b] | 3 | .108 | 2.648 | 3 | .115 | 2.6479 | $3^-$ |
| | | | | | | 2.6585 | $9^-$ |
| 2.78226[b] | 5 | .026 | 2.787 | | | 2.78226 | $5^-$ |
| 2.831±.005 | | | | | | 2.8264 | $(4^-,5^-)$ |
| 2.861±.005 | | | | | | 2.8646 | $7^-$ |
| 2.928[b] | 4 | .030 | 2.931 | | | 2.928 | $4^+$ |
| | | | | | | 2.9396 | $6^-$ |
| 2.960±.002 | | | | | | | |
| 2.988±.003 | | | | | | 2.979 | |
| 3.014±.003 | 5 | .016 | 3.020 | 5 | .021 | 3.01649 | $5^-$ |
| 3.033±.003 | | | | | | | |
| 3.121±.003 | $(J^\pi=3^+$[c]$)$ | | 3.124 | | | 3.122 | $(3^+)$ |
| 3.139±.006 | | | | | | | |
| 3.193±.003 | (5) | .011 | | | | 3.194 | |
| 3.224±.005 | | | | | | 3.2255 | $(6^-,7^-)$ |
| | | | | | | 3.2442 | $(4^-)$ |
| 3.257±.001 | 6 | .018 | 3.267 | | | | |

Table 1 continued

| Present Work | | | 65 MeV (p,p') Ref. 2 | | | Compilation Ref. 16 | |
|---|---|---|---|---|---|---|---|
| $E_x \pm \Delta E_x$ [a] | L | $\beta_L$ | $E_x$ [a] | L | $\beta_L$ | $E_x$ [a] | $J^\pi$ |
| 3.277±.001 | 5 | .015 | | | | 3.2793 | $5^-$ |
| 3.328±.005 | | | | | | | |
| 3.377±.002 | | | | | | 3.383 | $(7^-)$ |
| 3.399±.001 | 5 | .020 | 3.403 | 5 | .023 | 3.4028 | $5^-$ |
| 3.450±.001 | 4 | .020 | 3.453 | 3 | .019 | 3.453 | |
| 3.478±.004 | | | | | | 3.484 | |
| 3.515±.003 | (5) | .012 | | | | 3.519 | $(3^+,4^+)$ |
| 3.558±.002 | 5 | .022 | 3.560 | 5 | .024 | 3.5629 | $5^-$ |
| | | | | | | 3.595 | |
| 3.603±.004 | | | | | | 3.605 | |
| 3.655±.005 | | | | | | | |
| 3.675±.006 | | | | | | 3.676 | |
| 3.718±.002 | 3 | .023 | 3.721 | | | 3.722 | |
| 3.737±.004 | $(J^\pi=1^+$ [c]$)$ | | | | | 3.744 | $(1^+)$ |
| 3.772±.002 | 5 | .043 | 3.776 | 5 | .077 | 3.768 | $(5^-)$ |
| 3.795±.006 | | | | | | 3.791 | |
| 3.827±.005 | | | | | | 3.833 | |
| 3.847±.004 | | | | | | | |
| 3.883±.005 | | | | | | | |
| 3.898±.005 | | | | | | 3.902 | |
| | | | | | | 3.950 | |
| | | | | | | 3.9576 | $10^+$ |
| 3.963±.005 | (8) | .012 | | | | 3.963 | $(4^+)$ |
| 3.980±.005 | | | | | | | |
| 3.997±.005 | | | | | | 3.990 | |
| 4.006±.003 | (4) | .022 | 4.005 | | | 4.008 | $(4^+)$ |
| | | | | | | 4.0272 | $(12^+)$ |
| 4.044±.003 | (6,7) | .014,.016 | | | | 4.040 | |
| | | | | | | 4.055 | |
| 4.059±.005 | (5) | .014 | 4.075 | | | 4.067 | $(5^-)$ |
| 4.073±.007 | | | | | | | |
| | | | | | | 4.094 | |
| 4.107±.002 | 2 | 0.047 | 4.128 | 2 | .064 | 4.116 | $(2^+)$ |
| 4.123±.003 | 6 | .022 | | | | | |
| 4.145±.005 | | | | | | 4.150 | |
| 4.168±.004 | (3) | .009 | 4.191 | | | 4.162 | |
| 4.183±.005 | | | | | | | |

Table 1 continued

| Present Work | | | 24.5 MeV (p,p') Ref. 2 | | | Compilation Ref. 16 | |
|---|---|---|---|---|---|---|---|
| $E_x \pm \Delta E_x$ [a] | L | $\beta_L$ | $E_x$ [a] | L | $\beta_L$ | $E_x$ [a] | $J^\pi$ |
| 4.219±.003 | (4) | .017 | 4.259 | | | 4.218 | |
| 4.242±.003 | (2) | .016 | | | | 4.238 | $(5^-)$ |
| 4.292±.005 | (3) | .014 | | | | 4.292 | |
| | | | | | | 4.326 | (1) |
| | | | | | | 4.345 | $(6^+)$ |
| 4.333±.002 | 4 | .055 | 4.368 | 4 | .067 | 4.353 | $(4^+)$ |
| 4.357±.003 | 6 | .054 | 4.386 | 6 | .061 | 4.390 | $(6^+)$ |
| 4.391±.005 | (5) | .012 | | | | | |
| 4.420±.005 | | | | | | | |
| | | | | | | 4.430 | |
| 4.456±.005 | (5) | .020 | | | | | |
| 4.474±.003 | 5 | .016 | | | | 4.478 | |
| 4.496±.005 | (5,6) | .001,012 | | | | 4.492 | |
| 4.534±.004 | 5 | .016 | | | | 4.534 | |
| | | | | | | 4.555 | |
| 4.580±.003 | 8 | .033 | 4.600 | 8 | .045 | 4.602 | $(8^+)$ |

Table 2

| Present work | | | Present work | | | Present work | | |
|---|---|---|---|---|---|---|---|---|
| $E_x$ [a] $\pm \Delta E_x$ | L | $\beta_L$ | $E_x$ [a] $\pm \Delta E_x$ | L | $\beta_L$ | $E_x$ [a] $\pm \Delta E_x$ | L | $\beta_L$ |
| 4.595±.005 | | | 5.332±.007 | (3) | .011 | 6.023±.007 | | |
| 4.614±.007 | (3) | .004 | 5.365±.006 | | | 6.040±.005 | | |
| 4.647±.005 | | | 5.403±.006 | | | 6.065±.008 | | |
| 4.664±.004 | 5 | .011 | 5.422±.006 | (4) | .019 | 6.071±.004 | | |
| 4.691±.007 | | | 5.435±.007 | | | 6.083±.007 | | |
| 4.710±.004 | (4, 5) | .015, .016 | 5.452±.008 | (4) | .016 | 6.117±.007 | | |
| 4.729±.006 | | | 5.463±.006 | (3) | .014 | 6.146±.007 | | |
| 4.742±.005 | | | 5.485±.004 | (4) | .017 | 6.154±.005 | | |
| 4.770±.004 | | | 5.507±.006 | | | 6.167±.006 | | |
| 4.793±.005 | 5 | .022 | 5.533±.006 | (4) | .018 | 6.181±.007 | | |
| 4.809±.006 | (5, 6) | .013, .014 | 5.544±.007 | | | 6.198±.007 | (6) | .011 |
| 4.828±.004 | (7) | .023 | 5.561±.008 | (4) | .022 | 6.229±.008 | | |
| 4.860±.006 | (6) | .010 | 5.588±.008 | (5) | .020 | 6.264±.006 | (5) | .012 |
| 4.873±.004 | | | 5.599±.008 | | | 6.284±.008 | | |
| 4.889±.005 | (3) | .015 | 5.619±.008 | | | 6.302±.007 | | |
| 4.901±.004 | | | 5.640±.008 | (3) | .012 | 6.314±.006 | | |
| 4.916±.004 | (3) | .015 | 5.653±.008 | | | 6.332±.006 | | |
| 4.939±.004 | (6) | .020 | 5.676±.006 | | | 6.346±.006 | | |
| 4.960±.007 | (3) | .018 | 5.687±.004 | | | 6.382±.008 | | |
| 4.986±.003 | (3) | .018 | 5.703±.008 | (5) | .015 | 6.408±.008 | | |
| 5.007±.004 | (4) | .024 | 5.715±.007 | | | 6.433±.007 | | |
| 5.025±.005 | | | 5.722±.007 | | | 6.444±.007 | | |
| 5.045±.006 | | | 5.747±.008 | | | 6.459±.007 | | |
| 5.069±.006 | | | 5.763±.008 | | | 6.480±.007 | | |
| 5.092±.004 | (3, 4) | .013, .012 | 5.779±.008 | (5) | .014 | 6.496±.009 | | |
| 5.111±.005 | (4) | .015 | 5.796±.007 | (4, 5) | .014, .013 | 6.524±.009 | | |
| 5.126±.006 | (5) | .014 | 5.823±.008 | | | 6.545±.010 | | |
| 5.138±.007 | | | 5.843±.008 | | | 6.574±.008 | | |
| 5.169±.004 | | | 5.860±.007 | | | 6.593±.009 | | |
| 5.190±.005 | | | 5.885±.004 | | | 6.617±.008 | | |
| 5.209±.005 | | | 5.011±.007 | (4) | .023 | 6.634±.010 | | |
| 5.227±.008 | | | 5.949±.007 | | | 6.655±.008 | | |
| 5.245±.003 | (3) | .022 | 5.959±.005 | | | 6.689±.011 | | |
| 5.279±.005 | | | 5.974±.005 | | | 6.692±.007 | | |
| 5.296±.006 | | | 5.990±.008 | | | 6.761±.005 | | |
| 5.309±.004 | | | 6.001±.005 | | | 6.806±.006 | | |

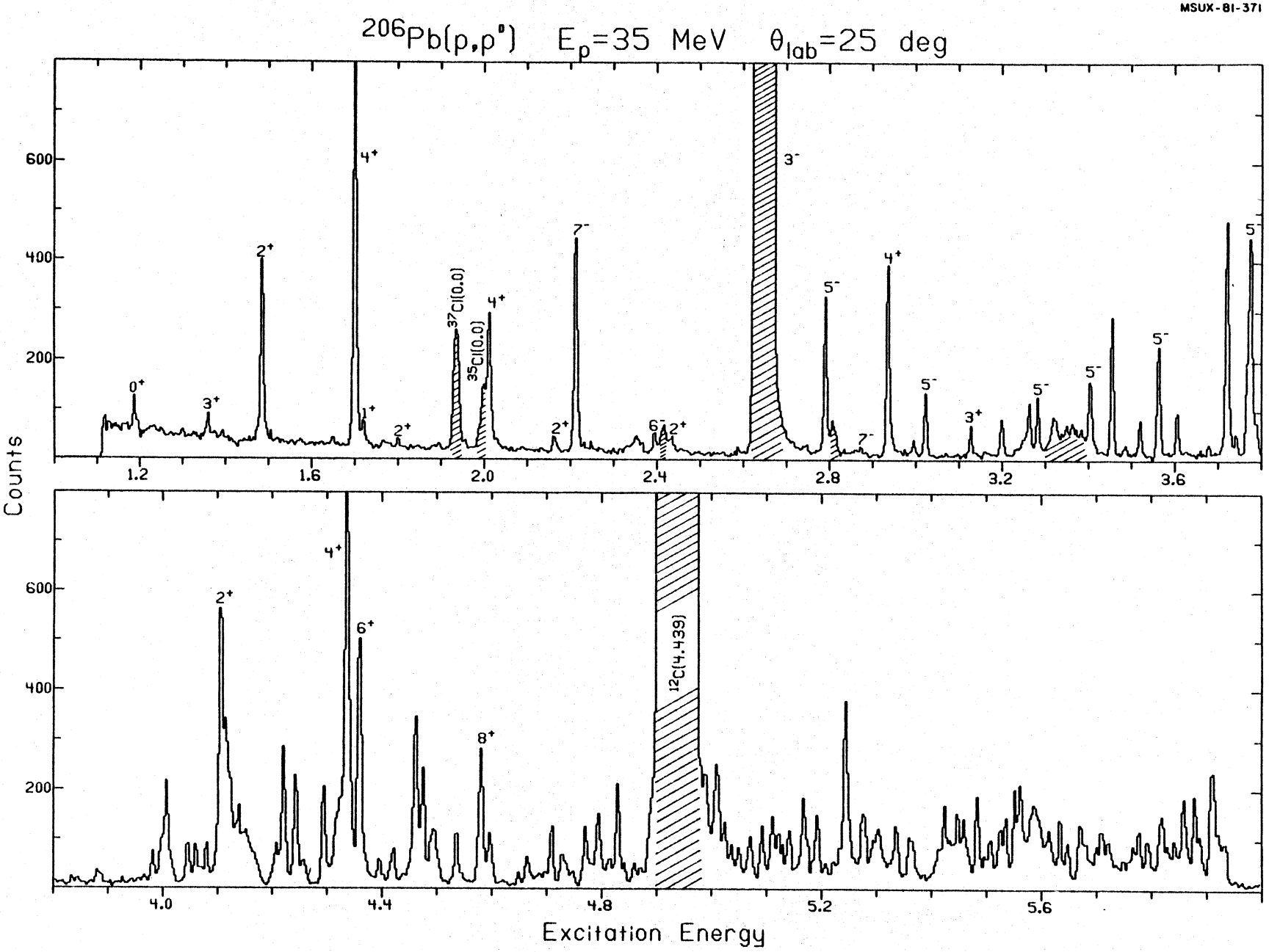
$^{206}$Pb(p,p$^{0}$) $E_p$=35 MeV $\theta_{lab}$=25 deg
Counts
Excitation Energy
0+
3+
2+
4+
1+
2+
37Cl(0.0)
35Cl(0.0)
4+
2+
7-
6-
2+
3-
5-
7-
4+
5-
3+
5-
5-
5-
5-
5-
2+
4+
6+
8+
12C(4.439)

Fig. 1. Typical spectrum of protons scattered by $^{206}Pb$ obtained with a photographic plate. States of well-determined spin and parity are identified. The resolution is about 6 keV.

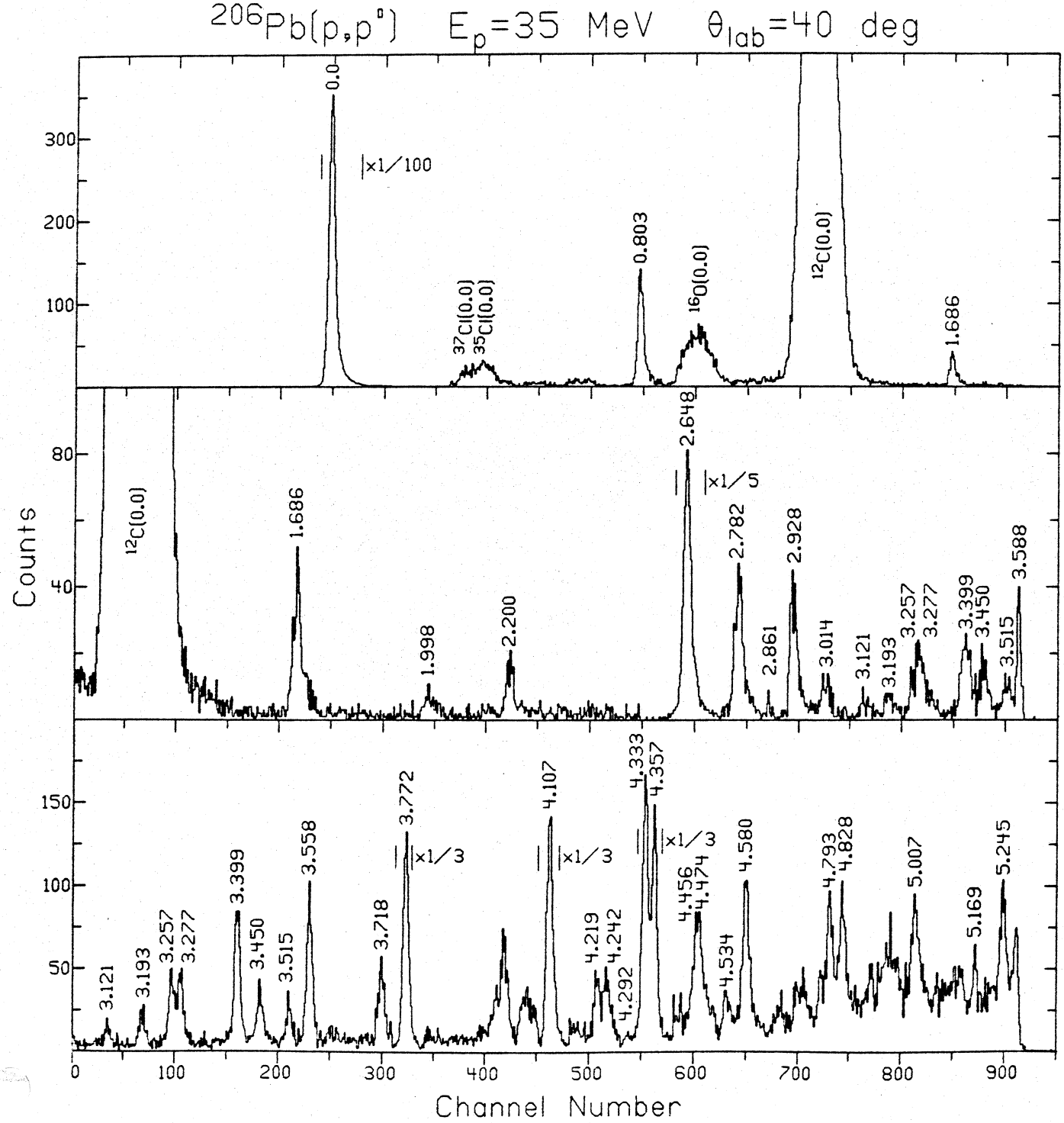
$^{206}$Pb(p,p$'$) $E_p$=35 MeV $\theta_{lab}$=40 deg
Counts
Channel Number
0.0
×1/100
0.803
$^{16}$O(0.0)
$^{37}$Cl(0.0)
$^{35}$Cl(0.0)
$^{12}$C(0.0)
1.686
1.998
2.200
2.648
×1/5
2.782
2.861
2.928
3.014
3.121
3.193
3.257
3.277
3.399
3.450
3.515
3.588
3.121
3.193
3.257
3.277
3.399
3.450
3.515
3.558
3.718
3.772
×1/3
4.107
×1/3
4.219
4.242
4.292
4.333
4.357
×1/3
4.456
4.474
4.534
4.580
4.793
4.828
5.007
5.169
5.245

Fig. 2. Typical spectrum of protons scattered by $^{206}Pb$ obtained with the proportional counter.

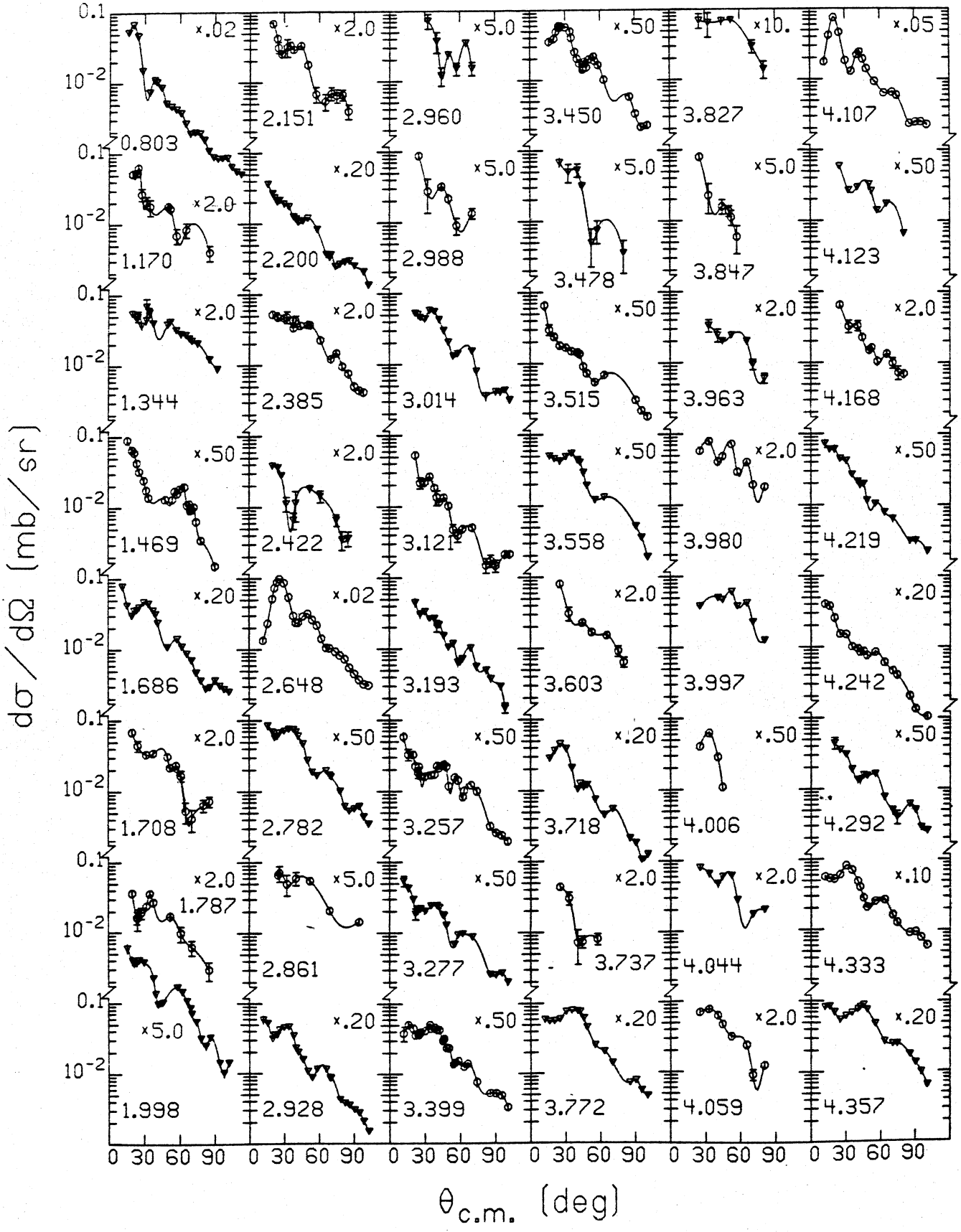
dσ / dΩ (mb/sr)
θc.m. (deg)
0.803
2.151
2.960
3.450
3.827
4.107
1.170
2.200
2.988
3.478
3.847
4.123
1.344
2.385
3.014
3.515
3.963
4.168
1.469
2.422
3.121
3.558
3.980
4.219
1.686
2.648
3.193
3.603
3.997
4.242
1.708
2.782
3.257
3.718
4.006
4.292
1.787
2.861
3.277
3.737
4.044
4.333
1.998
2.928
3.399
3.772
4.059
4.357

Fig. 3. Measured inelastic cross sections. The lines drawn through the data points are included to guide the eye and do not represent theoretical fits to the data.

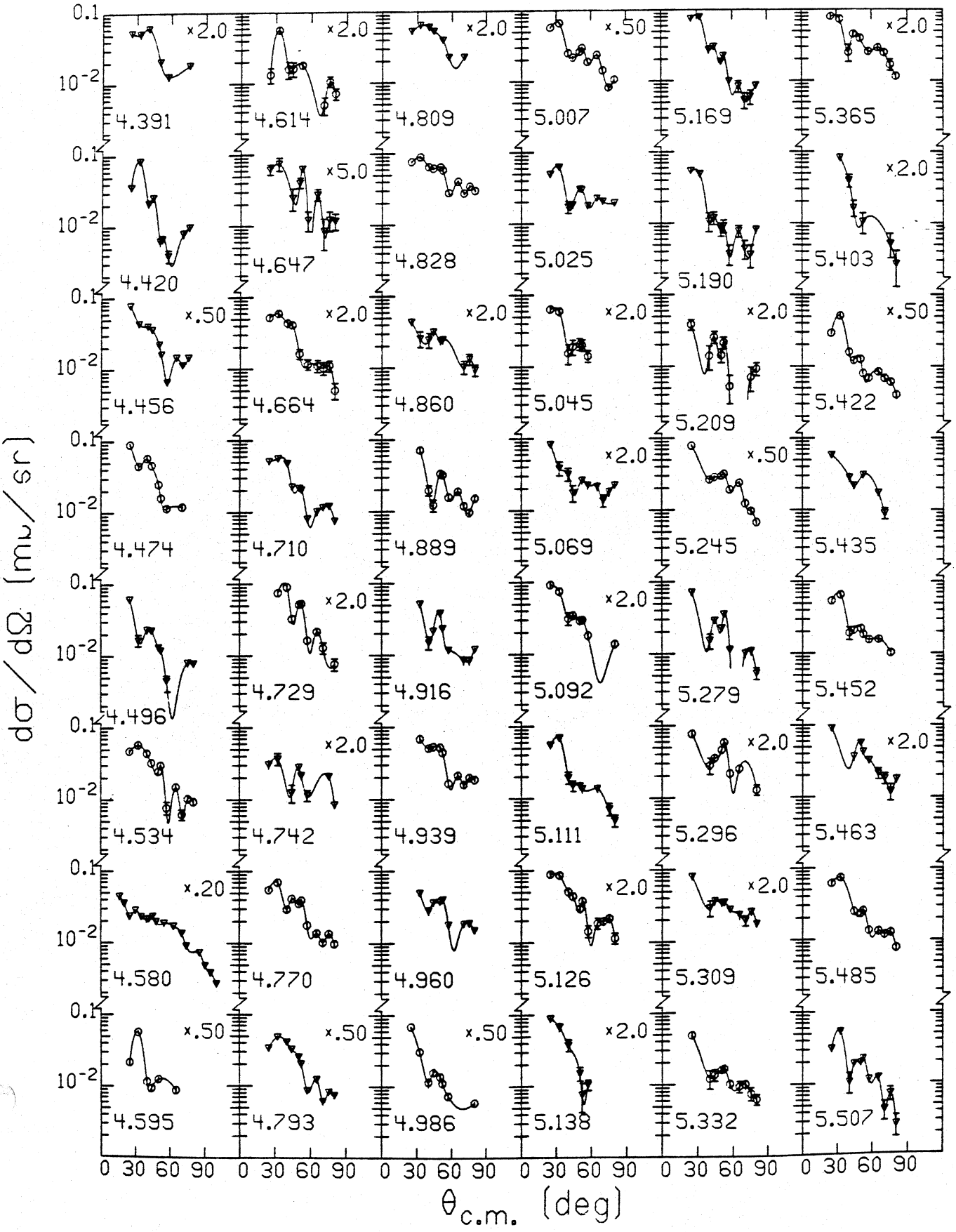
dσ/dΩ (mb/sr)
θc.m. (deg)
0.1
10-2
0 30 60 90
4.391
4.420
4.456
4.474
4.496
4.534
4.580
4.595
4.614
4.647
4.664
4.710
4.729
4.742
4.770
4.793
4.809
4.828
4.860
4.889
4.916
4.939
4.960
4.986
5.007
5.025
5.045
5.069
5.092
5.111
5.126
5.138
5.169
5.190
5.209
5.245
5.279
5.296
5.309
5.332
5.365
5.403
5.422
5.435
5.452
5.463
5.485
5.507
×2.0
×5.0
×.50
×.20

Fig. 4. Same as Fig. 3.

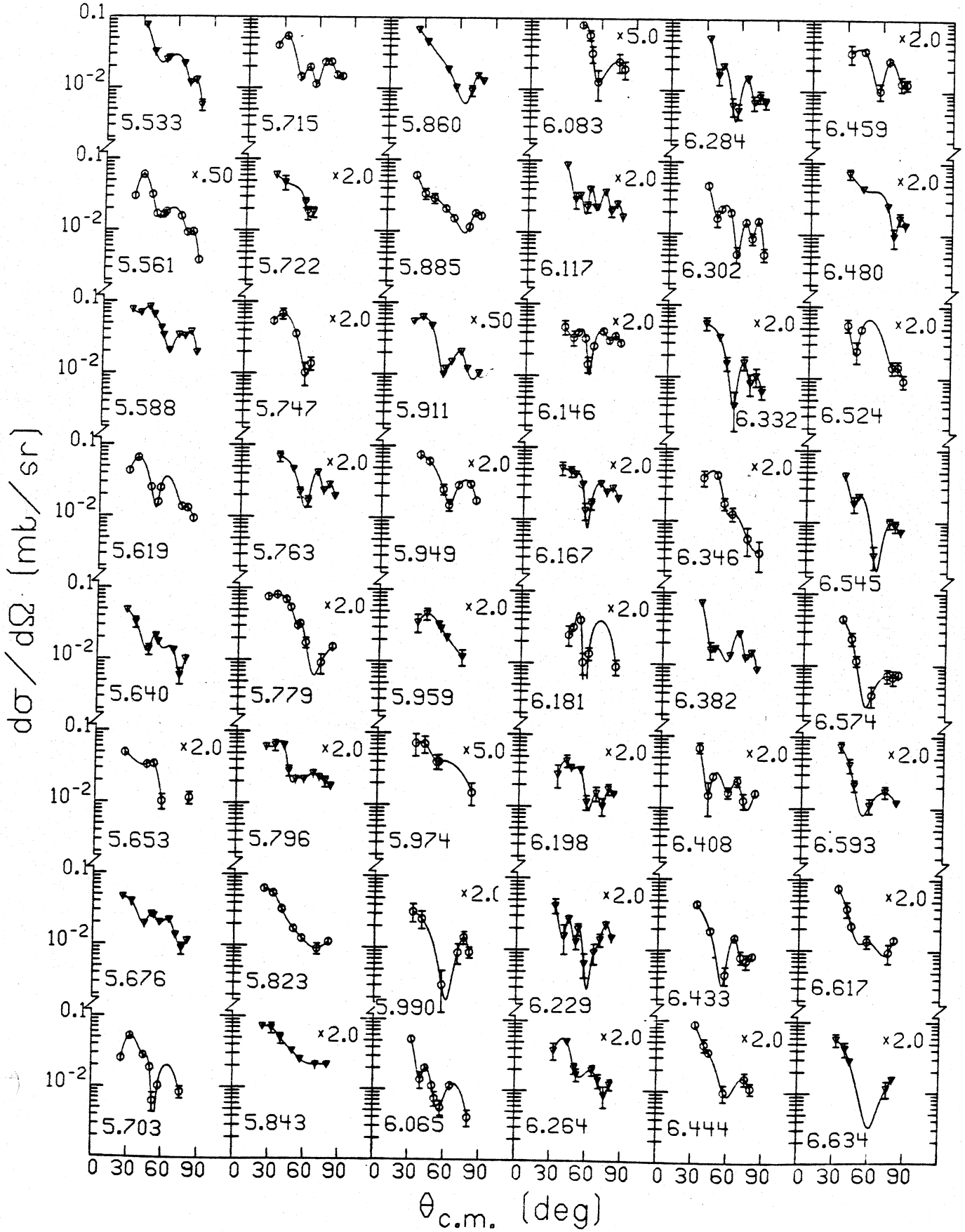
dσ/dΩ (mb/sr)
θc.m. (deg)
0 30 60 90
0.1
10-2
5.533
5.715
5.860
6.083
6.284
6.459
5.561
5.722
5.885
6.117
6.302
6.480
5.588
5.747
5.911
6.146
6.332
6.524
5.619
5.763
5.949
6.167
6.346
6.545
5.640
5.779
5.959
6.181
6.382
6.574
5.653
5.796
5.974
6.198
6.408
6.593
5.676
5.823
5.990
6.229
6.433
6.617
5.703
5.843
6.065
6.264
6.444
6.634

Fig. 5. Same as Fig. 3.

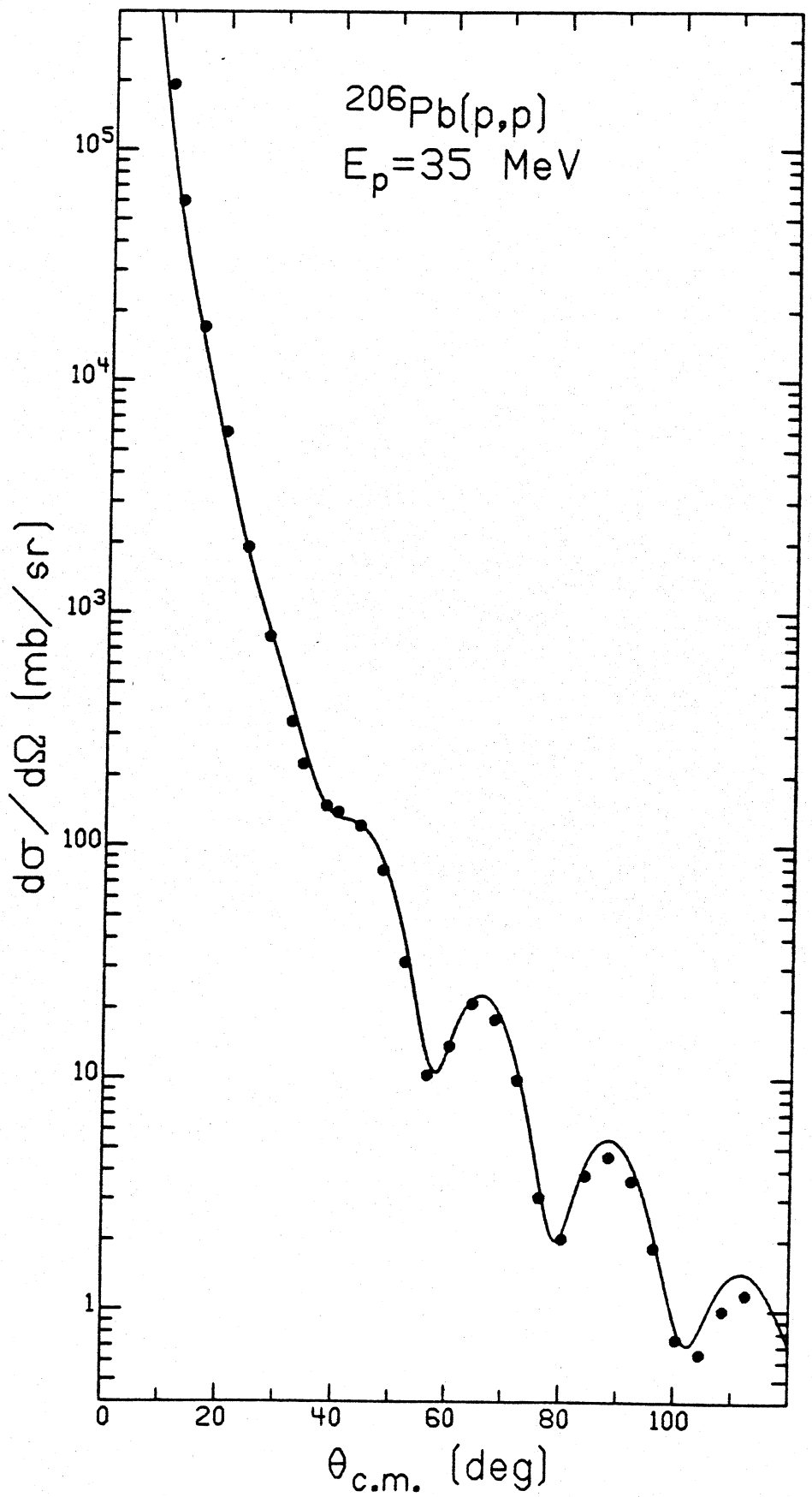
$^{206}$Pb(p,p)
$E_p$=35 MeV
$10^5$
$10^4$
$10^3$
100
10
1
dσ/dΩ (mb/sr)
0
20
40
60
80
100
$\theta_{c.m.}$ (deg)

Fig. 6. Comparison of the measured elastic angular distribution with the DWBA calculation explained in the text.

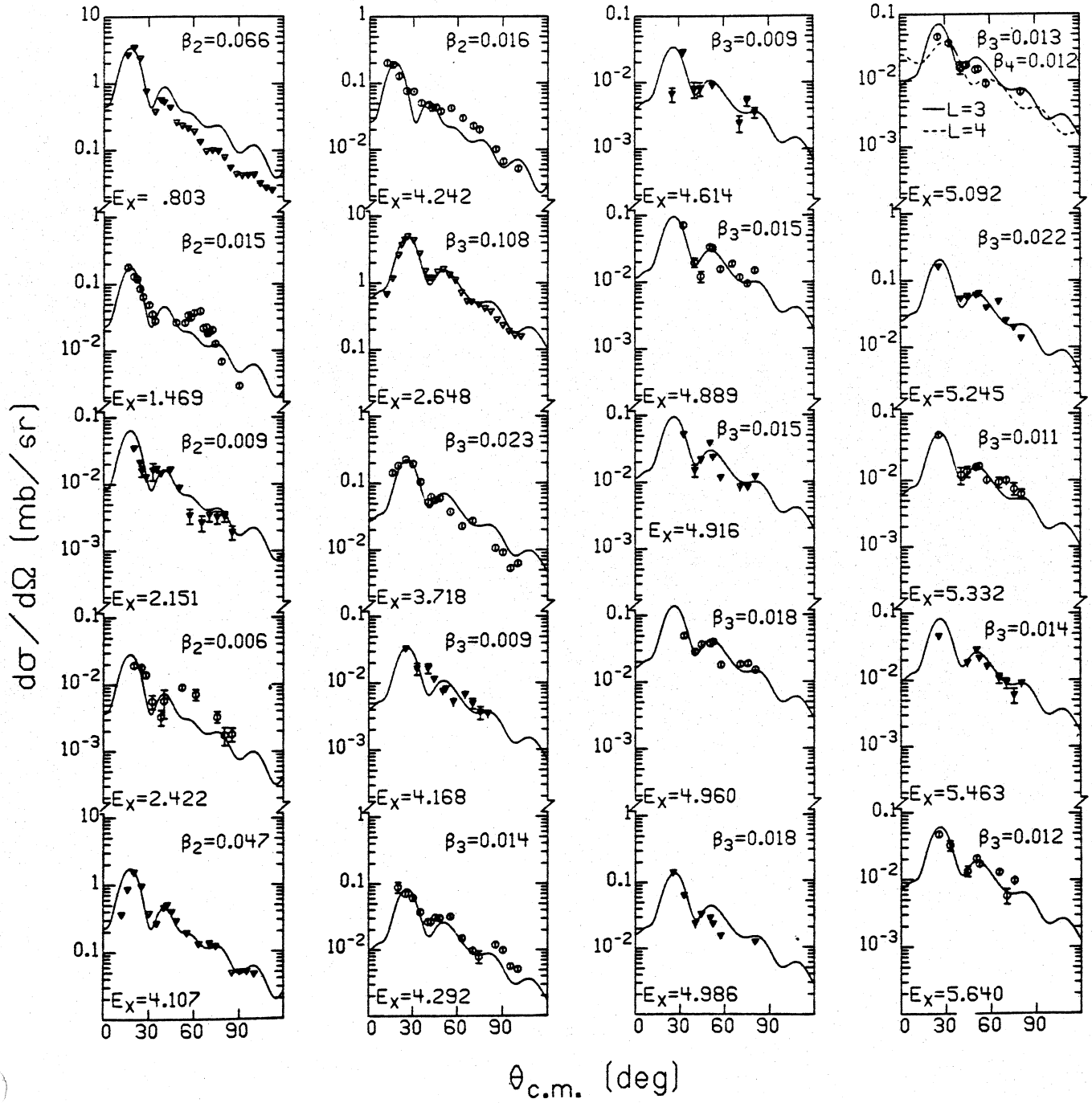
β2=0.066
Ex= .803
β2=0.015
Ex=1.469
β2=0.009
Ex=2.151
β2=0.006
Ex=2.422
β2=0.047
Ex=4.107
β2=0.016
Ex=4.242
β3=0.108
Ex=2.648
β3=0.023
Ex=3.718
β3=0.009
Ex=4.168
β3=0.014
Ex=4.292
β3=0.009
Ex=4.614
β3=0.015
Ex=4.889
β3=0.015
Ex=4.916
β3=0.018
Ex=4.960
β3=0.018
Ex=4.986
β3=0.013
β4=0.012
—L=3
---L=4
Ex=5.092
β3=0.022
Ex=5.245
β3=0.011
Ex=5.332
β3=0.014
Ex=5.463
β3=0.012
Ex=5.640
dσ/dΩ (mb/sr)
θc.m. (deg)

Fig. 7. Collective model fits for identified states. Displayed with each fit are the excitation energy of the state and the deformation parameter, $\beta_L$, corresponding to orbital angular momentum transfer L.

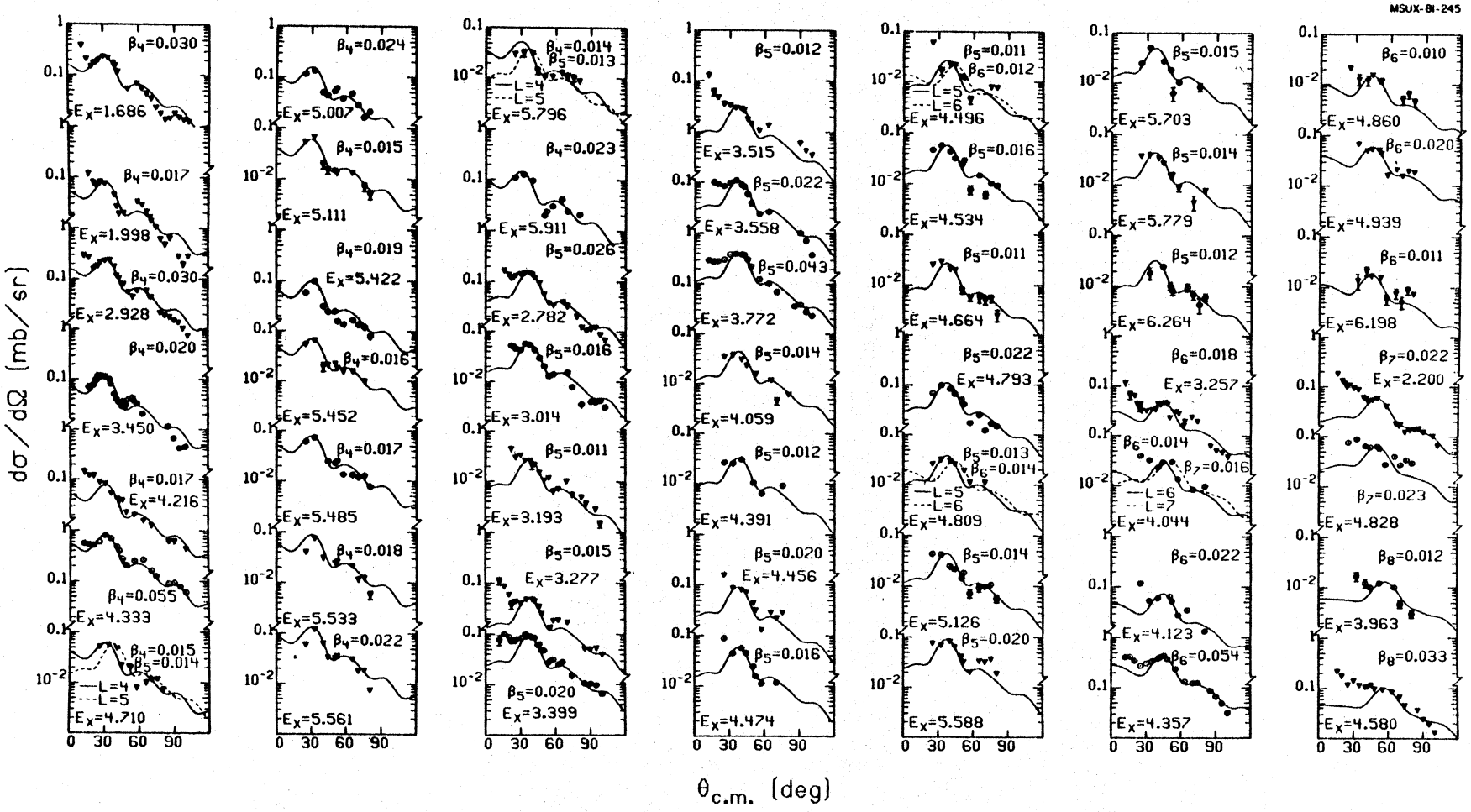
dσ/dΩ (mb/sr)
θc.m. (deg)
Ex=1.686
β4=0.030
Ex=1.998
β4=0.017
Ex=2.928
β4=0.030
Ex=3.450
β4=0.020
Ex=4.216
β4=0.017
Ex=4.333
β4=0.055
Ex=4.710
β4=0.015
β5=0.014
L=4
L=5
Ex=5.007
β4=0.024
Ex=5.111
β4=0.015
Ex=5.422
β4=0.019
Ex=5.452
β4=0.016
Ex=5.485
β4=0.017
Ex=5.533
β4=0.018
Ex=5.561
β4=0.022
Ex=5.796
β4=0.014
β5=0.013
L=4
L=5
Ex=5.911
β4=0.023
Ex=2.782
β5=0.026
Ex=3.014
β5=0.016
Ex=3.193
β5=0.011
Ex=3.277
β5=0.015
Ex=3.399
β5=0.020
Ex=3.515
β5=0.012
Ex=3.558
β5=0.022
Ex=3.772
β5=0.043
Ex=4.059
β5=0.014
Ex=4.391
β5=0.012
Ex=4.456
β5=0.020
Ex=4.474
β5=0.016
Ex=4.496
β5=0.011
β6=0.012
L=5
L=6
Ex=4.534
β5=0.016
Ex=4.664
β5=0.011
Ex=4.793
β5=0.022
Ex=4.809
β5=0.013
β6=0.014
L=5
L=6
Ex=5.126
β5=0.014
Ex=5.588
β5=0.020
Ex=4.044
β5=0.015
Ex=4.123
β6=0.022
Ex=4.357
β6=0.054
Ex=4.580
β6=0.010
Ex=4.860
β6=0.020
Ex=4.939
β6=0.011
Ex=5.703
β5=0.014
Ex=5.779
β5=0.012
Ex=6.198
β7=0.022
Ex=6.264
β6=0.018
Ex=3.257
β6=0.014
Ex=2.200
β7=0.016
L=6
L=7
β7=0.023
Ex=4.828
β8=0.012
Ex=3.963
β8=0.033
0 30 60 90

Fig. 8. Same as Fig. 7.

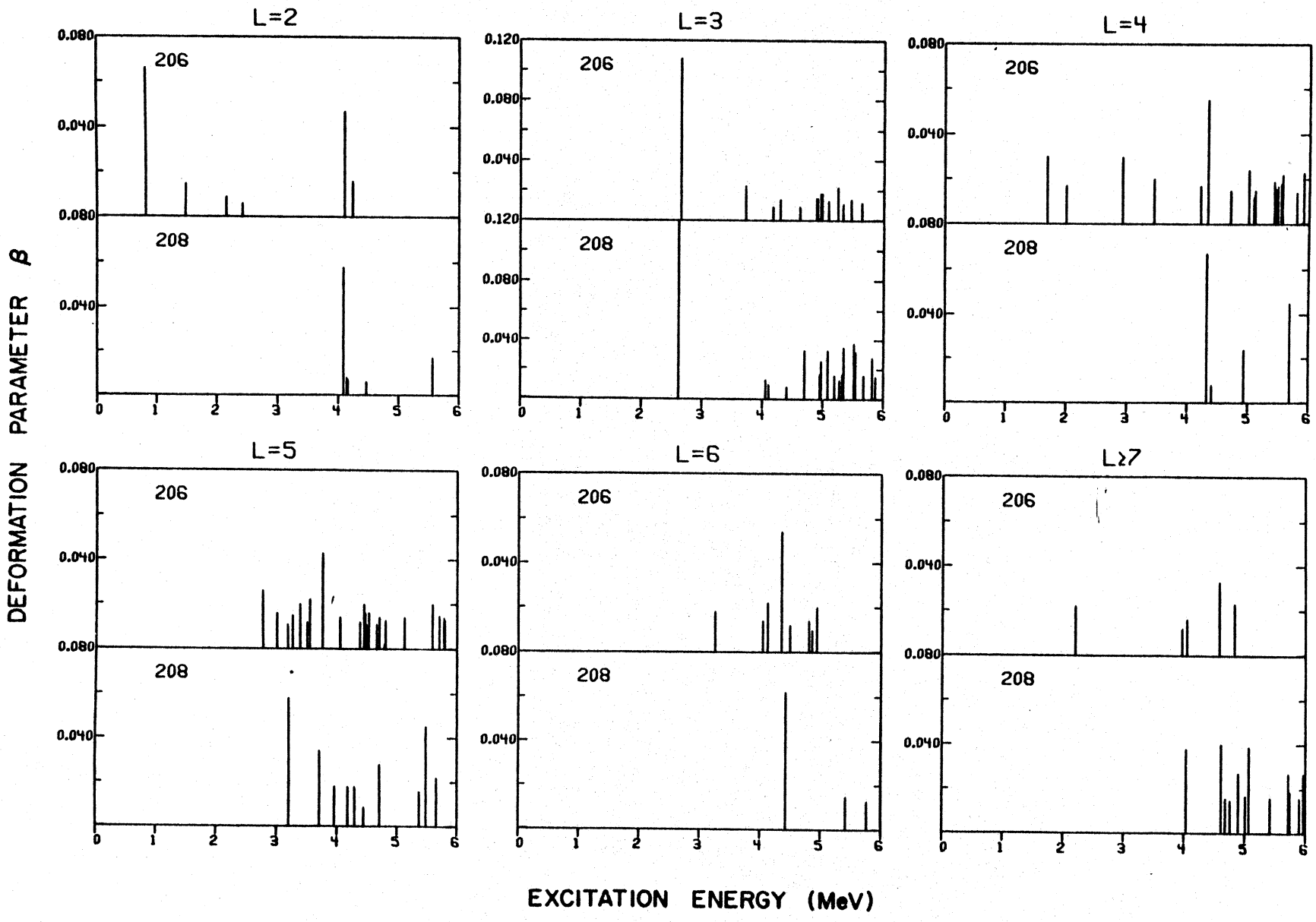
L=2
L=3
L=4
L=5
L=6
L≥7
206
208
DEFORMATION PARAMETER β
EXCITATION ENERGY (MeV)

Fig. 9. Results of collective model fits of $^{206}$Pb compared to $^{208}$Pb. The deformation parameter, $\beta_L$, is plotted against excitation energy for a number of L-transfers.

MSUX-82-127

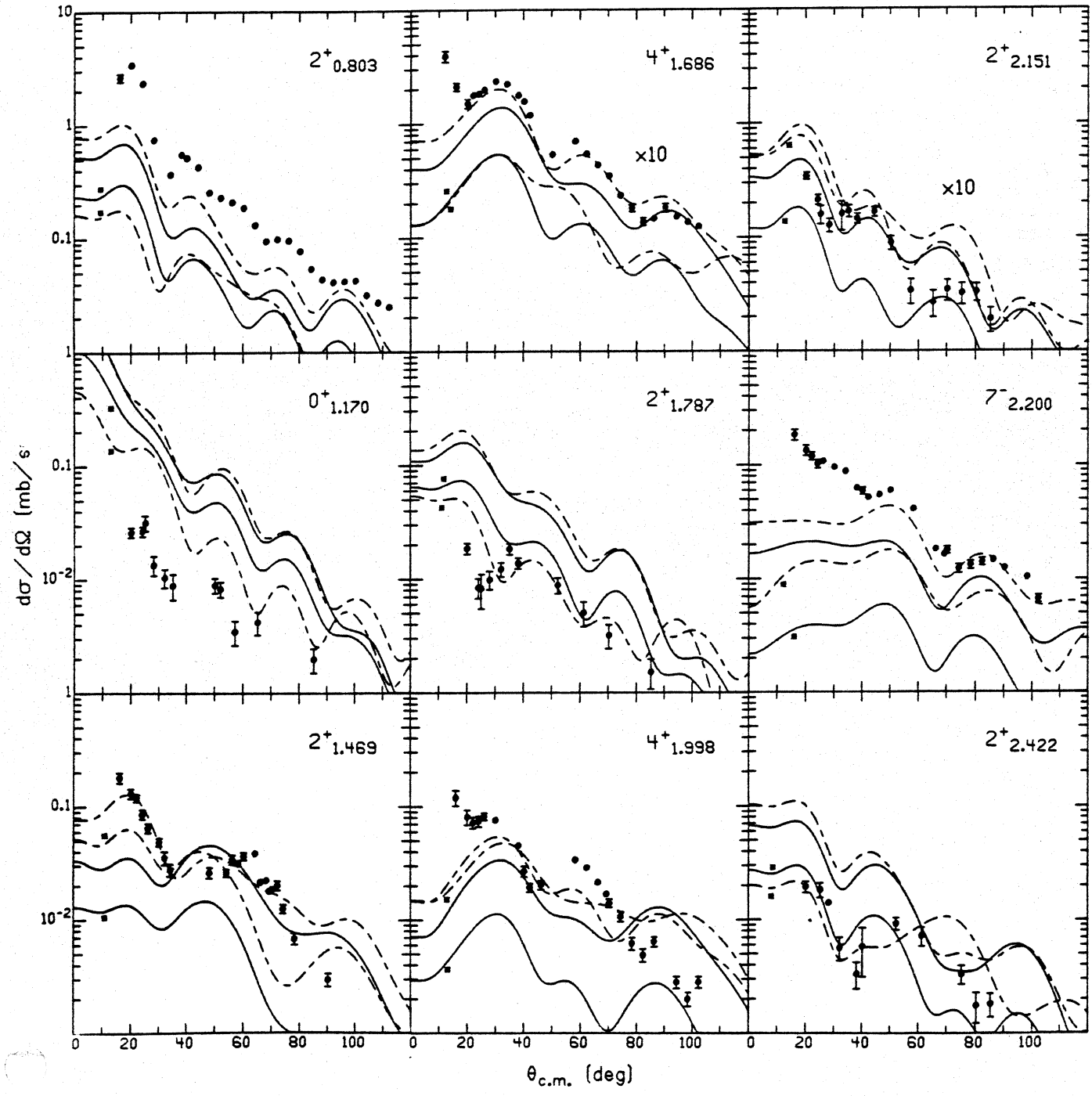
2+ 0.803
4+ 1.686
×10
2+ 2.151
×10
0+ 1.170
2+ 1.787
7- 2.200
2+ 1.469
4+ 1.998
2+ 2.422
dσ/dΩ (mb/sr)
θc.m. (deg)

Fig. 10. Microscopic model fits for low-lying natural parity states using RPA wave functions. The solid lines correspond to calculations done with Force A; the dashed curves show results using Force B. The asterisks indicate only direct calculations. The curves without asterisks indicate calculations including exchange effects.

MSUX-82-126

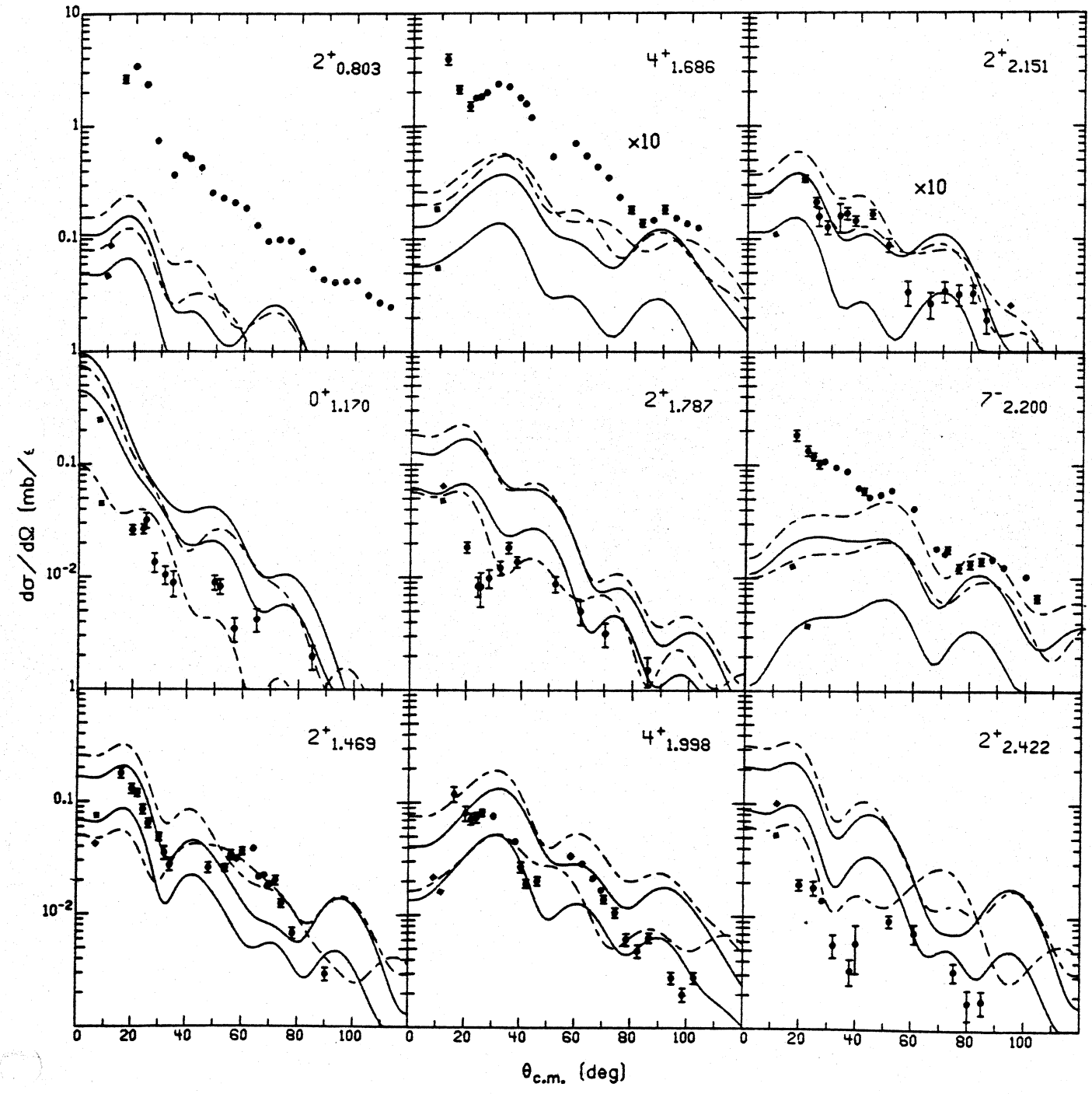
2+ 0.803
4+ 1.686
×10
2+ 2.151
×10
0+ 1.170
2+ 1.787
7- 2.200
2+ 1.469
4+ 1.998
2+ 2.422
dσ/dΩ (mb/ε)
θc.m. (deg)

Fig. 11. Same as Fig. 10 with TDA wave functions used in the calculations.

MSUX-81-265

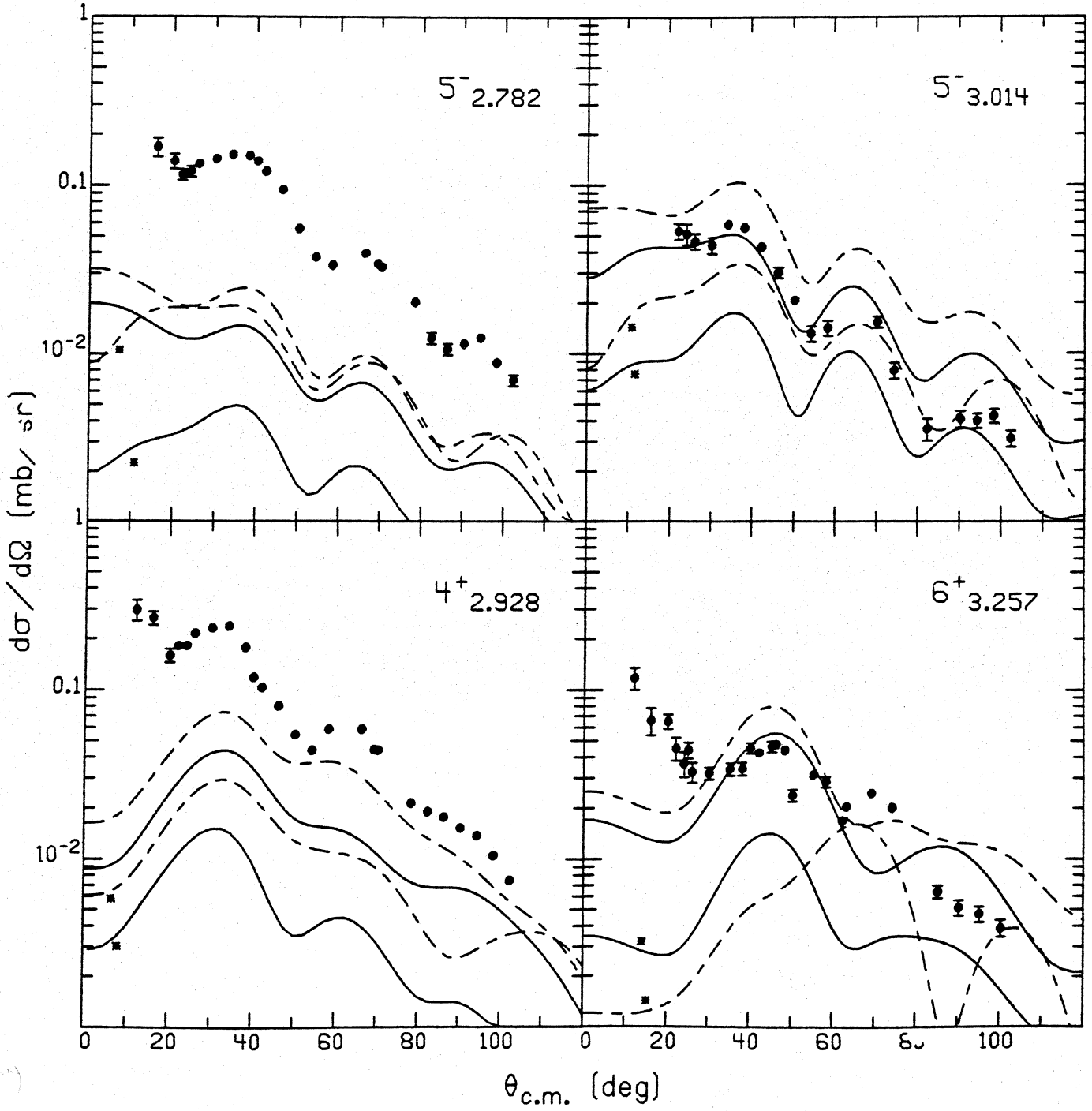
5⁻ 2.782
5⁻ 3.014
4⁺ 2.928
6⁺ 3.257
dσ/dΩ (mb/sr)
θc.m. (deg)
1
0.1
10⁻²
0
20
40
60
80
100

Fig. 12. Microscopic Model fits for higher-lying natural parity states using RPA wave functions. The meanings of the curves and asterisks are the same as in Fig. 10.

MSUX-81-266

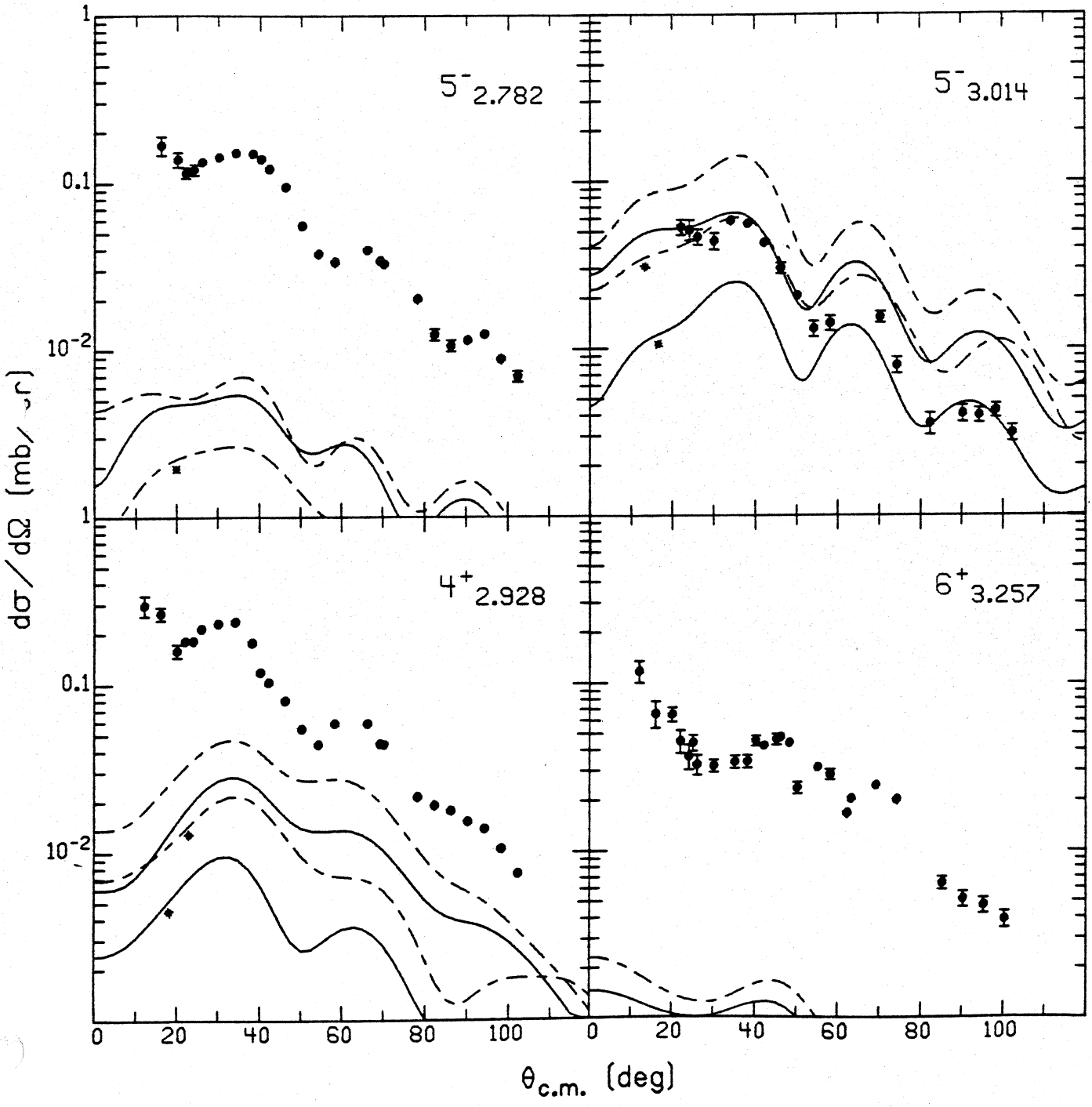
5⁻ 2.782
5⁻ 3.014
4⁺ 2.928
6⁺ 3.257
dσ/dΩ (mb/sr)
θc.m. (deg)
1
0.1
10⁻²
0
20
40
60
80
100

Fig. 13. Same as Fig. 12 with TDA wave functions used in the calculations.

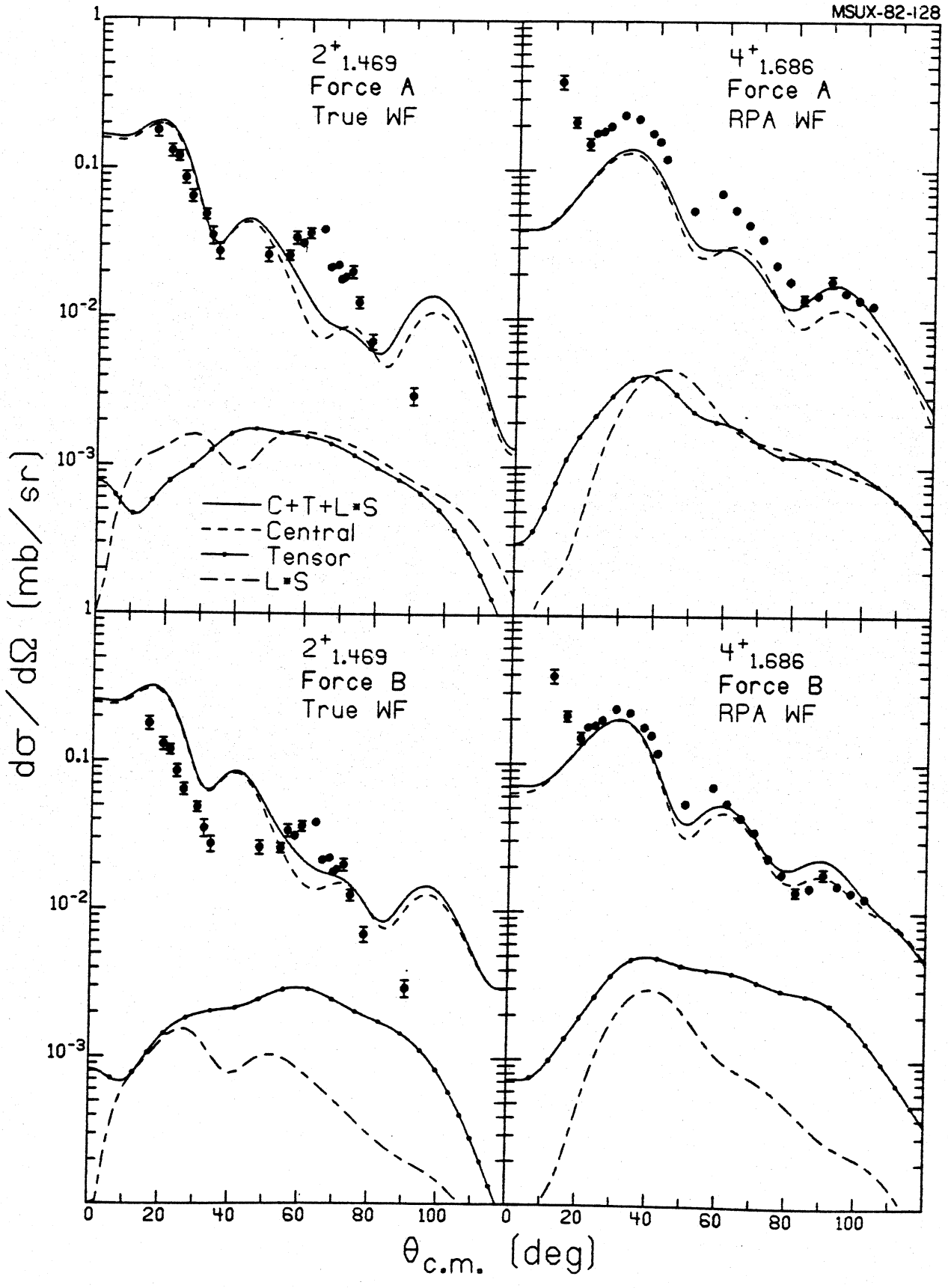
MSUX-82-128
2+ 1.469
Force A
True WF
4+ 1.686
Force A
RPA WF
2+ 1.469
Force B
True WF
4+ 1.686
Force B
RPA WF
C+T+L•S
Central
Tensor
L•S
dσ/dΩ (mb/sr)
θc.m. (deg)
1
0.1
10-2
10-3
0
20
40
60
80
100

Fig. 14. Comparison of measured angular distributions with the central and noncentral parts of Force A and Force B.

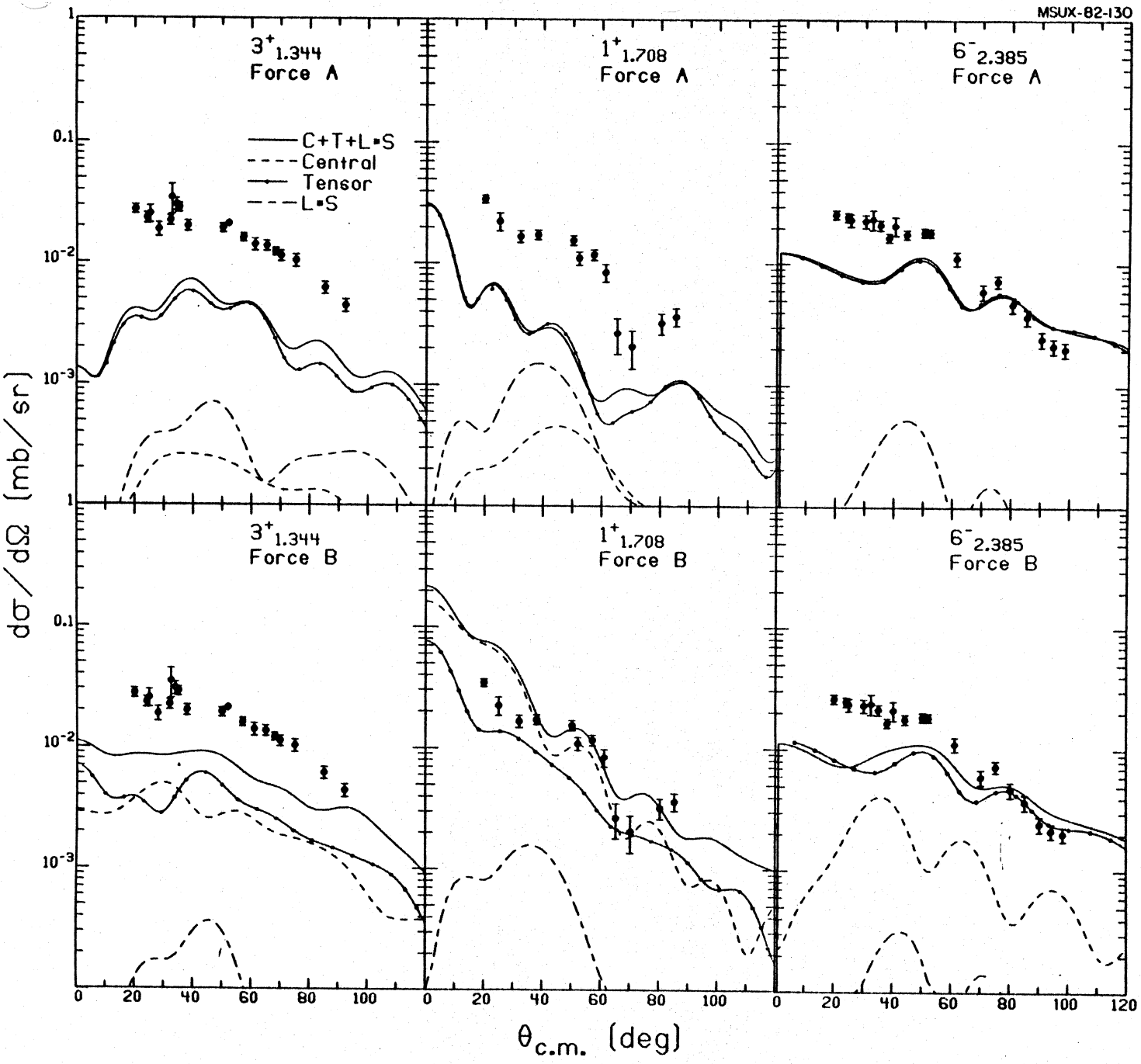
MSUX-82-130
$3^+_{1.344}$ Force A
$1^+_{1.708}$ Force A
$6^-_{2.385}$ Force A
C+T+L•S
Central
Tensor
L•S
$3^+_{1.344}$ Force B
$1^+_{1.708}$ Force B
$6^-_{2.385}$ Force B
dσ/dΩ (mb/sr)
$\theta_{c.m.}$ (deg)

Fig. 15. Same as Fig. 14.

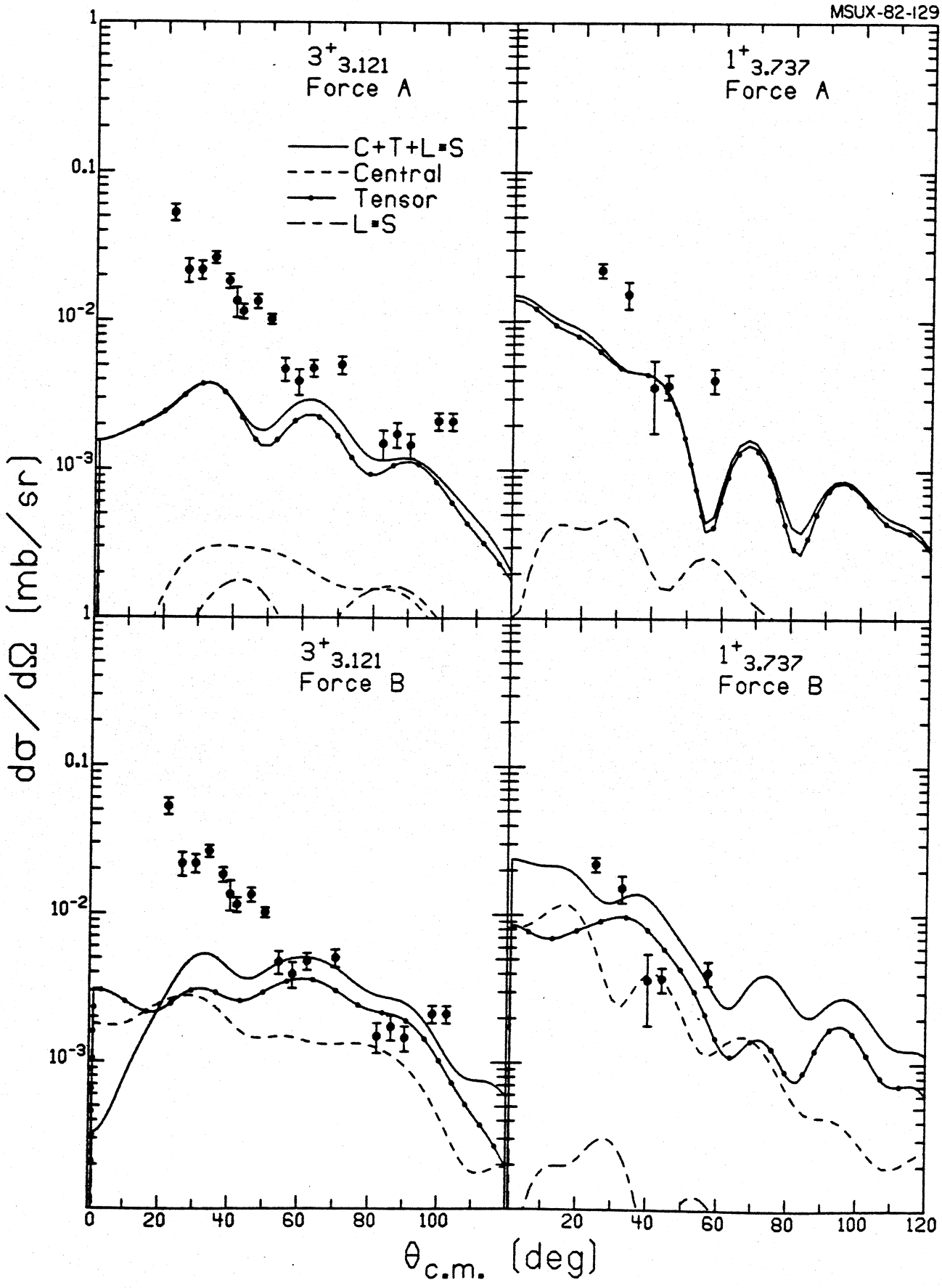
MSUX-82-129
3+ 3.121
Force A
C+T+L·S
Central
Tensor
L·S
1+ 3.737
Force A
3+ 3.121
Force B
1+ 3.737
Force B
dσ/dΩ (mb/sr)
θc.m. (deg)

Fig. 16. Same as Fig. 14.

| Present Work | | | 24.5 MeV (p,p') Ref. 2 | | | Compilation Ref. 16 | |
|---|---|---|---|---|---|---|---|
| $E_x \pm \Delta E_x$ [a] | L | $\beta_L$ | $E_x$ [a] | L | $\beta_L$ | $E_x$ [a] | $J^\pi$ |
| 0.00[b] | | | | | | 0.00 | $0^+$ |
| 0.8031[b] | 2 | .066 | 0.803 | 2 | .068 | 0.8031 | $2^+$ |
| 1.170±.003 | | | | | | 1.1651 | $0^+$ |
| 1.344±.002 | $J^\pi=3^+$ [c] | | 1.328 | | | 1.3406 | $3^+$ |
| 1.469±.002 | 2 | .015 | 1.459 | | | 1.467 | $2^+$ |
| 1.686±.001 | 4 | .030 | 1.684 | 4 | .042 | 1.6841 | $4^+$ |
| 1.708±.003 | $J^\pi=1^+$ [c] | | | | | 1.703 | $1^+$ |
| 1.787±.002 | | | 1.789 | | | 1.784 | $2^+$ |
| 1.9977[b] | 4 | .017 | 1.996 | 4 | .023 | 1.9977 | $4^+$ |
| 2.151±.003 | (2) | .009 | | | | 2.149 | $(2^+)$ |
| 2.20023[b] | 7 | .022 | 2.199 | 7 | .031 | 2.20023 | $7^-$ |
| | | | | | | 2.315 | $0^+$ |
| | | | | | | 2.379 | |
| 2.385±.002 | $J^\pi=6^-$ [c] | | 2.381 | | | 2.3843 | $6^-$ |
| | | | | | | 2.3914 | |
| 2.422±.003 | (2) | .006 | | | | 2.424 | $2^+$ |
| 2.6479[b] | 3 | .108 | 2.648 | 3 | .115 | 2.6479 | $3^-$ |
| | | | | | | 2.6585 | $9^-$ |
| 2.78226[b] | 5 | .026 | 2.787 | | | 2.78226 | $5^-$ |
| 2.831±.005 | | | | | | 2.8264 | $(4^-,5^-)$ |
| 2.861±.005 | | | | | | 2.8646 | $7^-$ |
| 2.928[b] | 4 | .030 | 2.931 | | | 2.928 | $4^+$ |
| | | | | | | 2.9396 | $6^-$ |
| 2.960±.002 | | | | | | | |
| 2.988±.003 | | | | | | 2.979 | |
| 3.014±.003 | 5 | .016 | 3.020 | 5 | .021 | 3.01649 | $5^-$ |
| 3.033±.003 | | | | | | | |
| 3.121±.003 | $(J^\pi=3^+$ [c]$)$ | | 3.124 | | | 3.122 | $(3^+)$ |
| 3.139±.006 | | | | | | | |
| 3.193±.003 | (5) | .011 | | | | 3.194 | |
| 3.224±.005 | | | | | | 3.2255 | $(6^-,7^-)$ |
| | | | | | | 3.2442 | $(4^-)$ |
| 3.257±.001 | 6 | .018 | 3.267 | | | | |

Table 1. Energy levels, L-transfers, and deformation parameters for $^{206}Pb$. A comparison is made with previous results.

a. All energies are in MeV.
b. Level used in energy calibration.
c. Spin and parity adopted from Ref. 16.

Table 1 Continued

| Present Work | | | 24.5 MeV (p,p') Ref. 2 | | | Compilation Ref. 16 | |
|---|---|---|---|---|---|---|---|
| $E_x \pm \Delta E_x$ [a] | L | $\beta_L$ | $E_x$ [a] | L | $\beta_L$ | $E_x$ [a] | $J^\pi$ |
| 3.277±.001 | 5 | .015 | | | | 3.2793 | $5^-$ |
| 3.328±.005 | | | | | | | |
| 3.377±.002 | | | | | | 3.383 | $(7^-)$ |
| 3.399±.001 | 5 | .020 | 3.403 | 5 | .023 | 3.4028 | $5^-$ |
| 3.450±.001 | 4 | .020 | 3.453 | 3 | .019 | 3.453 | |
| 3.478±.004 | | | | | | 3.484 | |
| 3.515±.003 | (5) | .012 | | | | 3.519 | $(3^+,4^+)$ |
| 3.558±.002 | 5 | .022 | 3.560 | 5 | .024 | 3.5629 | $5^-$ |
| | | | | | | 3.595 | |
| 3.603±.004 | | | | | | 3.605 | |
| 3.655±.005 | | | | | | | |
| 3.675±.006 | | | | | | 3.676 | |
| 3.718±.002 | 3 | .023 | 3.721 | | | 3.722 | |
| 3.737±.004 | $(J^\pi=1^+$ [c]$)$ | | | | | 3.744 | $(1^+)$ |
| 3.772±.002 | 5 | .043 | 3.776 | 5 | .077 | 3.768 | $(5^-)$ |
| 3.795±.006 | | | | | | 3.791 | |
| 3.827±.005 | | | | | | 3.833 | |
| 3.847±.004 | | | | | | | |
| 3.883±.005 | | | | | | | |
| 3.898±.005 | | | | | | 3.902 | |
| | | | | | | 3.950 | |
| | | | | | | 3.9576 | $10^+$ |
| 3.963±.005 | (8) | .012 | | | | 3.963 | $(4^+)$ |
| 3.980±.005 | | | | | | | |
| 3.997±.005 | | | | | | 3.990 | |
| 4.006±.003 | (4) | .022 | 4.005 | | | 4.008 | $(4^+)$ |
| | | | | | | 4.0272 | $(12^+)$ |
| 4.044±.003 | (6,7) | .014,.016 | | | | 4.040 | |
| | | | | | | 4.055 | |
| 4.059±.005 | (5) | .014 | 4.075 | | | 4.067 | $(5^-)$ |
| 4.073±.007 | | | | | | | |
| | | | | | | 4.094 | |
| 4.107±.002 | 2 | 0.047 | 4.128 | 2 | .064 | 4.116 | $(2^+)$ |
| 4.123±.003 | 6 | .022 | | | | | |
| 4.145±.005 | | | | | | 4.150 | |
| 4.168±.004 | (3) | .009 | 4.191 | | | 4.162 | |
| 4.183±.005 | | | | | | | |

Table 1 Continued

| Present Work | | | 24.5 MeV (p,p') Ref. 2 | | | Compilation Ref. 16 | |
|---|---|---|---|---|---|---|---|
| $E_x \pm \Delta E_x$ [a] | L | $\beta_L$ | $E_x$ [a] | L | $\beta_L$ | $E_x$ [a] | $J^\pi$ |
| 4.219±.003 | (4) | .017 | 4.259 | | | 4.218 | |
| 4.242±.003 | (2) | .016 | | | | 4.238 | $(5^-)$ |
| 4.292±.005 | (3) | .014 | | | | 4.292 | |
| | | | | | | 4.326 | (1) |
| | | | | | | 4.345 | $(6^+)$ |
| 4.333±.002 | 4 | .055 | 4.368 | 4 | .067 | 4.353 | $(4^+)$ |
| 4.357±.003 | 6 | .054 | 4.386 | 6 | .061 | 4.390 | $(6^+)$ |
| 4.391±.005 | (5) | .012 | | | | | |
| 4.420±.005 | | | | | | | |
| | | | | | | 4.430 | |
| 4.456±.005 | (5) | .020 | | | | | |
| 4.474±.003 | 5 | .016 | | | | 4.478 | |
| 4.496±.005 | (5,6) | .001,012 | | | | 4.492 | |
| 4.534±.004 | 5 | .016 | | | | 4.534 | |
| | | | | | | 4.555 | |
| 4.580±.003 | 8 | .033 | 4.600 | 8 | .045 | 4.602 | $(8^+)$ |

Table 2

| Present work | | | Present work | | | Present work | | |
|---|---|---|---|---|---|---|---|---|
| $E_x$ [a] $\pm \Delta E_x$ | L | $\beta_L$ | $E_x$ [a] $\pm \Delta E_x$ | L | $\beta_L$ | $E_x$ [a] $\pm \Delta E_x$ | L | $\beta_L$ |
| [illegible].595±.005 | | | 5.332±.007 | (3) | .011 | 6.023±.007 | | |
| 4.614±.007 | (3) | .004 | 5.365±.006 | | | 6.040±.005 | | |
| 4.647±.005 | | | 5.403±.006 | | | 6.065±.008 | | |
| 4.664±.004 | 5 | .011 | 5.422±.006 | (4) | .019 | 6.071±.004 | | |
| 4.691±.007 | | | 5.435±.007 | | | 6.083±.007 | | |
| 4.710±.004 | (4, 5) | .015, .016 | 5.452±.008 | (4) | .016 | 6.117±.007 | | |
| 4.729±.006 | | | 5.463±.006 | (3) | .014 | 6.146±.007 | | |
| 4.742±.005 | | | 5.485±.004 | (4) | .017 | 6.154±.005 | | |
| 4.770±.004 | | | 5.507±.006 | | | 6.167±.006 | | |
| 4.793±.005 | 5 | .022 | 5.533±.006 | (4) | .018 | 6.181±.007 | | |
| 4.809±.006 | (5, 6) | .013, .014 | 5.544±.007 | | | 6.198±.007 | (6) | .011 |
| 4.828±.004 | (7) | .023 | 5.561±.008 | (4) | .022 | 6.229±.008 | | |
| 4.860±.006 | (6) | .010 | 5.588±.008 | (5) | .020 | 6.264±.006 | (5) | .012 |
| 4.873±.004 | | | 5.599±.008 | | | 6.284±.008 | | |
| 4.889±.005 | (3) | .015 | 5.619±.008 | | | 6.302±.007 | | |
| 4.901±.004 | | | 5.640±.008 | (3) | .012 | 6.314±.006 | | |
| [illegible].916±.004 | (3) | .015 | 5.653±.008 | | | 6.332±.006 | | |
| [illegible].939±.004 | (6) | .020 | 5.676±.006 | | | 6.346±.006 | | |
| 4.960±.007 | (3) | .018 | 5.687±.004 | | | 6.382±.008 | | |
| 4.986±.003 | (3) | .018 | 5.703±.008 | (5) | .015 | 6.408±.008 | | |
| 5.007±.004 | (4) | .024 | 5.715±.007 | | | 6.433±.007 | | |
| 5.025±.005 | | | 5.722±.007 | | | 6.444±.007 | | |
| 5.045±.006 | | | 5.747±.008 | | | 6.459±.007 | | |
| 5.069±.006 | | | 5.763±.008 | | | 6.480±.007 | | |
| 5.092±.004 | (3, 4) | .013, .012 | 5.779±.008 | (5) | .014 | 6.496±.009 | | |
| 5.111±.005 | (4) | .015 | 5.796±.007 | (4, 5) | .014, .013 | 6.524±.009 | | |
| 5.126±.006 | (5) | .014 | 5.823±.008 | | | 6.545±.010 | | |
| 5.138±.007 | | | 5.843±.008 | | | 6.574±.008 | | |
| 5.169±.004 | | | 5.860±.007 | | | 6.593±.009 | | |
| 5.190±.005 | | | 5.885±.004 | | | 6.617±.008 | | |
| 5.209±.005 | | | 5.011±.007 | (4) | .023 | 6.634±.010 | | |
| 5.227±.008 | | | 5.949±.007 | | | 6.655±.008 | | |
| 5.245±.003 | (3) | .022 | 5.959±.005 | | | 6.689±.011 | | |
| [illegible].279±.005 | | | 5.974±.005 | | | 6.692±.007 | | |
| [illegible].296±.006 | | | 5.990±.008 | | | 6.761±.005 | | |
| 5.309±.004 | | | 6.001±.005 | | | 6.806±.006 | | |

Table 2. Energy levels, L-transfers, and deformation parameters for $^{206}Pb$.

a. All energies are in MeV.